

Universality in Kinetic Models of Circadian Rhythms in *Arabidopsis thaliana*

Yian Xu,^{*} Masoud Asadi-Zeydabadi,[†] Randall Tagg,[†] and Orrin Shindell[‡]
(Dated: September 17, 2021)

Biological evolution has endowed the plant *Arabidopsis thaliana* with genetically regulated circadian rhythms. A number of authors have published kinetic models for these oscillating chemical reactions based on a network of interacting genes. To investigate the hypothesis that the *Arabidopsis* circadian dynamical system is poised near a Hopf bifurcation like some other biological oscillators, we varied the kinetic parameters in the models and searched for bifurcations. Finding that each model does exhibit a supercritical Hopf bifurcation, we performed a weakly nonlinear analysis near the bifurcation points to derive the Stuart-Landau amplitude equation. To illustrate a common dynamical structure, we scaled the numerical solutions to the models with the asymptotic solutions to the Stuart-Landau equation to collapse the circadian oscillations onto two universal curves – one for amplitude, and one for frequency. However, some models are close to bifurcation while others are far, some models are post-bifurcation while others are pre-bifurcation, and kinetic parameters that lead to a bifurcation in some models do not lead to a bifurcation in others. Future kinetic modeling can make use of our analysis to ensure models are consistent with each other and with the dynamics of the *Arabidopsis* circadian rhythm.

Keywords: Circadian Rhythms, *Arabidopsis thaliana*, Hopf Bifurcation, Stuart-Landau Equation

I. INTRODUCTION

Adapting to the 24-hour light-dark cycle caused by the rotation of the Earth, plants have evolved endogenous circadian rhythms that control many of their biological functions [1]. Circadian rhythms are genetically regulated chemical reactions inside cells that cause chemical concentrations to rise and fall with daily periodicity. Over the past fifteen years, eleven papers have proposed chemical kinetic models to govern the circadian oscillations in the laboratory plant *Arabidopsis thaliana* [2–12]. These sets of differential equations specify gene-interactions that were deduced through genetic experiments and include chemical reaction rate constants that were estimated by fits to experimental time series data [13–15].

As knowledge about the genetic regulation of circadian rhythms has increased, the models have become larger and more complicated: the original model of a two-gene feedback loop has seven differential equations and 28 parameters [2], while the largest model of 12 genes has 35 differential equations with 122 parameters [9]. Recent efforts have aimed to reduce the mathematical complexity of these models while retaining their dynamical features [11, 12, 16, 17].

Another body of literature studying circadian rhythms in *Arabidopsis* has focused on the spatiotemporal patterns formed when the genetic expression of individual cells are coupled together in the tissues of a live plant [18–24]. Some studies employed phenomenological mod-

els like the Stuart-Landau amplitude equation [18] and the related Kuramoto coupled phase oscillator model [22, 24, 25]. These coarse-grained descriptions are useful because they reduce the complicated dynamics of interacting gene networks with many rate constants to simple dynamical forms that contain only one or a few parameters. The parameters can then be fit to experimental results, a process recently proposed as a tool in agricultural engineering projects [26].

In the present work, we employ a weakly nonlinear analysis method, the *Reductive Perturbation Method* (RPM) of Kuramoto [25], to cast the *Arabidopsis* models into a two-dimensional form that is universally valid in systems poised near a Hopf bifurcation. The success of this approach is based on the fact that the published models are situated near supercritical Hopf bifurcation points in parameter space, a fact that may have biological significance: a nonlinear oscillator tuned near a Hopf bifurcation exhibits a resonance response when it is forced near its natural frequency [27, 28]. This mechanism confers sensitivity to some other biological oscillators, like the hair cells of the cochlea in the ears of humans [29, 30] and frogs [31].

Near a Hopf bifurcation, the nonlinear equations governing the chemical oscillations may be linearized about a fixed point to give an approximate two-dimensional oscillating solution with a complex amplitude. The complex amplitude is governed by the Stuart-Landau equation whose parameter values are derived from a higher order expansion of the nonlinear system, and are therefore functions of the rate constants without free parameters [25, 32, 33].

We perform the RPM calculation on the published circadian rhythms models for two reasons. The first is to show how to calculate the parameters appearing in the Stuart-Landau equation directly from the kinetic rate constants in the chemical kinetic models. This calculation suggests experimental routes to drive bifurcations in

^{*} Trinity University, Physics & Astronomy, San Antonio, Texas, 78212, United States

[†] University of Colorado Denver, Physics, Denver, Colorado, 80203, United States

[‡] oshindel@trinity.edu; Trinity University, Physics & Astronomy, San Antonio, Texas, 78212, United States

circadian rhythms by manipulating kinetic parameters, a useful method in pattern formation experiments and plant engineering projects. The second reason is to quantify the essential dynamical features that models should aim to capture in addition to the oscillation period: the eigenvalues of the linearized system indicate whether the model is post-bifurcation or pre-bifurcation; the dependence of the eigenvalues on the kinetic rate constants show which rate constants lead to bifurcation; and the error between the perturbation solution and numerical solution to the full kinetic equations provides a measure of the proximity of the model to Hopf bifurcation. These dynamical quantities should be consistent between models and with the circadian rhythms of the organism.

Our paper is organized into two sections. In the Methods and Results section we summarize the *Reductive Perturbation Method* and show how to apply it to one of the circadian rhythms models. Then we illustrate the universal structure underlying the kinetic models. Finally, in the Discussion we point out inconsistencies between the kinetic models and suggest experimental and modeling approaches that could give additional information about the chemical dynamics of the *Arabidopsis* circadian rhythm.

II. METHODS AND RESULTS

A. Hopf Bifurcations in the Circadian Rhythms Models

The *Arabidopsis* circadian rhythms models we considered are sets of coupled, nonlinear, first-order, ordinary differential equations. All of these models explicitly incorporate time dependence as a 24-hour periodic function. To investigate the dynamics of the endogenous chemical oscillations, we chose to make the differential equations autonomous by assuming perpetual darkness [16] or perpetual illumination [20]. The autonomous equations may be expressed in the general form,

$$\frac{d\mathbf{x}}{dt} = \mathbf{f}(\mathbf{x}; \mu) \quad (1)$$

where \mathbf{x} is an n -dimensional vector of chemical concentrations associated with the circadian reactions, \mathbf{f} is a nonlinear n -dimensional vector-valued function specifying the chemical reactions in a model, and μ is a function of one of the rate constants in the reaction equations. Using the kinetic rate constants as bifurcation parameters differs from previous work that studied time delay models for circadian rhythms and used the time delay constant as a Hopf bifurcation parameter [34].

Each of the circadian rhythms models we studied exhibits a supercritical Hopf bifurcation. Near $\mu = 0$, with μ suitably defined, the system of equations Eq. (1) possesses a fixed point, i.e., a constant solution \mathbf{X}_0 that satisfies

$$\mathbf{f}(\mathbf{X}_0; \mu) = \mathbf{0} \quad (2)$$

At the bifurcation point $\mu = 0$, the fixed point switches linear stability: in the pre-bifurcation region $\mu < 0$, \mathbf{X}_0 is stable, and in the post-bifurcation region $\mu > 0$, \mathbf{X}_0 is unstable. When the system is post-bifurcation, in addition to an unstable fixed point, it possesses a stable limit cycle, i.e., a linearly stable periodic solution $\mathbf{X}(t)$ that satisfies

$$\frac{d\mathbf{X}}{dt} = \mathbf{f}(\mathbf{X}; \mu), \quad \mathbf{X}(t) = \mathbf{X}(t + T) \quad (3)$$

for some period T . The limit-cycle dynamics near a Hopf bifurcation belong to a dynamical universality class: for $\mu \gtrsim 0$, the amplitude of the limit cycle oscillations scales in proportion to $\sqrt{\mu}$ and the frequency in proportion to μ . These properties enable an approximation to the amplitude and frequency of the limit cycle that is valid near the bifurcation point.

For a concrete example from the literature, we consider here the original model (L2005a) presented in Locke *et al.* [2], which assumes a single negative feedback interaction between two core circadian genes: *LATE ELONGATED HYPO-COTYL (LHY)*, which is partially redundant with *CIRCADIAN CLOCK ASSOCIATED 1*, and *TIMING OF CAB EXPRESSION 1 (TOC1)* [35]. A bifurcation diagram for L2005a is displayed in Fig. 1(f) in Tokuda *et al.* [16], which used the set of reaction rates given in the caption of Fig. 4 of Locke *et al.* [2]. We use this same parameter set in the analysis presented in this subsection and the next. As the transcription rate of *LHY* is varied in perpetual darkness, a supercritical Hopf bifurcation occurs.

In Fig. 1a, we compare the bifurcation diagram for the levels of *LHY* mRNA calculated analytically with RPM (discussed in more detail in the next subsection) to the numerical solution obtained using the differential equation solver MATLAB ODE15s [36]. The *LHY* transcription rate is normalized so that a value of unity corresponds to the fitted parameter value 7.5038 nM/h [16]. In Fig. 1b, we compare the frequency of oscillations calculated analytically with the results obtained numerically. At the biological value of the *LHY* transcription rate, the RPM calculation matches the amplitude and frequency determined by the numerical solution to the system of differential equations to within 0.86% for the amplitude and 0.45% for the frequency. In the Supplementary Materials, we show bifurcation diagrams for concentration and frequency of the other post-bifurcation models; as a measure of how close each model is poised to bifurcation we calculate the percent differences in amplitude and frequency between the numerical calculation and the RPM calculation at the fitted parameter values reported for each model.

B. Reductive Perturbation Method and the Stuart-Landau Amplitude Equation

In dynamical systems that undergo a Hopf bifurcation, an approximate two-dimensional periodic solution,

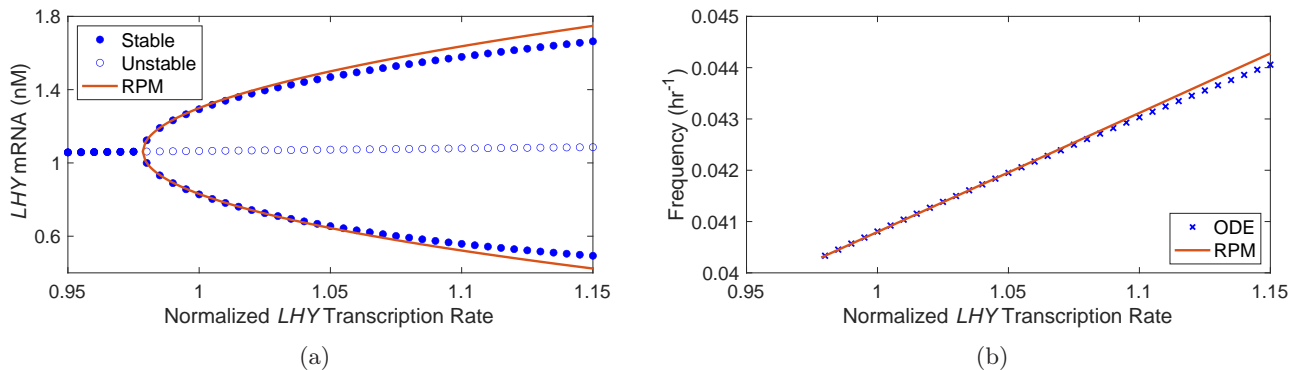


FIG. 1: Bifurcation in (a) concentration and (b) frequency of circadian oscillations in a model (L2005a) poised near a supercritical Hopf bifurcation. The transcription rate of *LHY* is normalized such that the estimated biological value is unity; the bifurcation occurs at 0.9785. (a) The central branch is the fixed point, which is stable to the left of 0.9785 (closed circles) and unstable to the right (open circles). The upper and lower branches are the maximum and minimum values of *LHY* mRNA limit cycle oscillations, calculated numerically (closed blue circles) and perturbatively (orange line). (b) The limit cycle frequency is calculated numerically (blue hash marks) and perturbatively (orange line).

valid near the bifurcation point, may be derived [25, 32]. This stems from the fact that one pair of complex conjugate eigenvalues of the Jacobian matrix have positive real parts, while all the other eigenvalues have negative real parts. The two eigenmodes associated with the former dominate the long-time behavior of the system, as the modes associated with the latter decay to zero.

The system of equations Eq. (1) may be linearized about the fixed point \mathbf{X}_0 , to give

$$\frac{d\mathbf{u}}{dt} = \mathbf{L}\mathbf{u}, \quad \mathbf{u} = \mathbf{x} - \mathbf{X}_0, \quad L_{ij} = \left. \frac{\partial f_i}{\partial x_j} \right|_{(\mathbf{x}_0, \mu)} \quad (4)$$

where \mathbf{u} is the deviation from the fixed point and \mathbf{L} is the Jacobian matrix. At the bifurcation point $\mu = 0$, the Jacobian matrix possesses n eigenvalues with n associated eigenvectors (the systems we studied had no repeated eigenvalues), with two of the eigenvalues purely imaginary. Thus, at bifurcation,

$$\mathbf{L}_0 \mathbf{U} = i\omega_0 \mathbf{U} \quad (5)$$

where \mathbf{L}_0 is the Jacobian matrix evaluated at $\mu = 0$ and \mathbf{U} is the eigenvector corresponding to the eigenvalue $i\omega_0$, with the complex conjugate eigenvector $\bar{\mathbf{U}}$ corresponding to the eigenvalue $-i\omega_0$. Near the bifurcation point in the post-bifurcation region, the linearized system has two eigenvalues with positive real parts that dominate the dynamics of system, as the remaining $n - 2$ eigenvalues have strictly negative real parts. There is the approximate eigenvalue equation

$$(\mathbf{L}_0 + \mu \mathbf{L}_1) \mathbf{U} = (i\omega_0 + \mu \lambda_1) \mathbf{U}, \quad \lambda_1 = \sigma_1 + i\omega_1, \quad \sigma_1 > 0 \quad (6)$$

where \mathbf{L}_1 is the first-order term of the Taylor expansion of \mathbf{L} about $\mu = 0$, and λ_1 is the first-order term in the Taylor series about $\mu = 0$ of the eigenvalue of \mathbf{L} whose

zeroth-order term is $i\omega_0$, with σ_1 the real part and ω_1 the imaginary part. For $\mu \gtrsim 0$, the solution $\mathbf{x}(t)$ takes the approximate form

$$\mathbf{x} = \mathbf{X}_0 + \sqrt{\mu} [W(t)\mathbf{U}e^{i\omega_0 t} + \bar{W}(t)\bar{\mathbf{U}}e^{-i\omega_0 t}] \quad (7)$$

where W is a complex amplitude, with \bar{W} the complex conjugate, that evolves according to the Stuart-Landau equation

$$\frac{dW}{dt} = \mu (\lambda_1 W - g|W|^2 W), \quad g = g' + ig'', \quad g' > 0 \quad (8)$$

The complex number g is a function of the higher order expansion coefficients of Eq. (1). We refer to Kuramoto [25] for the details leading to Eqs. (7) and (8). Eq. (8) can be split into two equations by setting $W(t) = R(t)e^{i\Theta(t)}$, with $R(t)$ and $\Theta(t)$ both real, which lead to the asymptotic quantities

$$R_s \equiv \lim_{t \rightarrow \infty} R = \sqrt{\frac{\sigma_1}{g'}}, \quad (9)$$

$$\omega_s \equiv \lim_{t \rightarrow \infty} \frac{d\Theta}{dt} = (\omega_1 - g'' R_s^2)$$

The limit cycle in the post-bifurcation region is thus approximately given by

$$\mathbf{X} = \mathbf{X}_0 + \sqrt{\mu} R_s [\mathbf{U}e^{i(\omega_0 + \mu\omega_s)t} + \bar{\mathbf{U}}e^{-i(\omega_0 + \mu\omega_s)t}] \quad (10)$$

which describes an elliptical orbit in a two-dimensional subspace of \mathbb{R}^n . In Fig. 2a, we compare the time series given by the limit cycle prediction of Eq. (10) to the numerically computed solution for the mRNA concentration of the central gene *LHY*.

The phase differences between different chemical species in the circadian system, which are important to

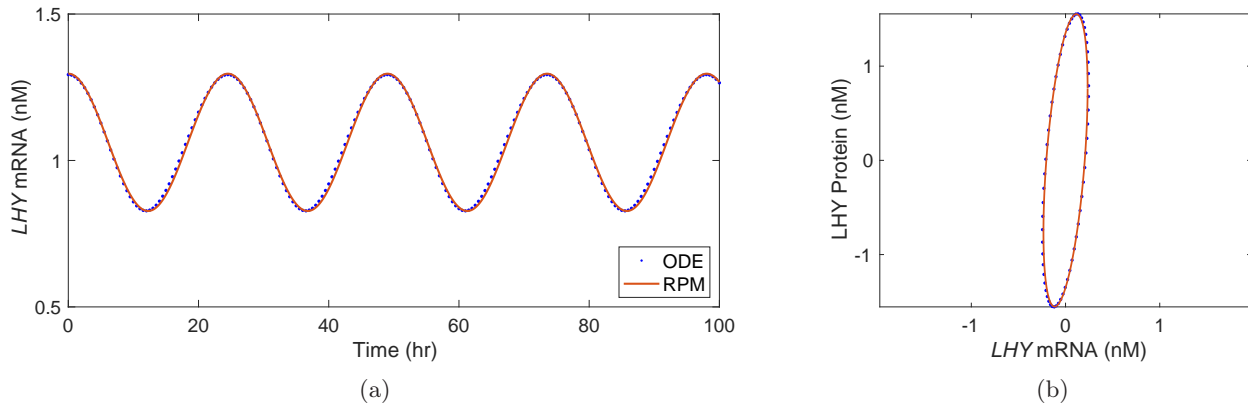


FIG. 2: Time series (a) and phase space plot (b) are calculated numerically (ODE) and perturbatively (RPM) for a model (L2005a) poised near a supercritical Hopf bifurcation.

biological function [2], can be estimated directly from the eigenvector \mathbf{U} . In Fig. 2b, we plot phase space diagrams for LHY protein and *LHY* mRNA oscillations. The phase difference between the pair of chemical species deviates from those obtained from numerical solutions; as a fraction of 2π the absolute value of the difference in phase difference is 0.003. In the Supplementary Materials, we show time series and phase space plots for the other post-bifurcation models.

C. Scaling and Data Collapse

The parameters appearing in the Stuart-Landau equation, which result from the values of the kinetic rate parameters in the circadian reactions, set natural scales for the chemical oscillations in the circadian rhythms models. Exactly at the bifurcation point, the system exhibits zero amplitude oscillations about the fixed point \mathbf{X}_0 with frequency ω_0 . As the system deviates from the bifurcation point with increasing μ , the limit cycle amplitudes of the oscillating chemicals increase in proportion $\sqrt{\mu}R_s$ while their frequency changes from ω_0 by $\mu\omega_s$. There is an arbitrariness in the calculation of these parameters, however, as the eigenvectors in Eq. (5) are unique only up to a multiplicative constant. To set an exact scale, we chose to normalize the eigenvectors by the component with the largest modulus, which sets $\sqrt{\mu}2R_s$ as an upper bound for the chemical oscillation amplitudes. With this definition, Eq. (10) implies that the amplitude A and frequency ω for the largest amplitude chemical species in the limit cycle regime can be collapsed onto parameter-free curves near $\mu = 0$:

$$\begin{aligned} \frac{A}{2R_s} &= \sqrt{\mu}, \\ \frac{\omega - \omega_0}{\omega_s} &= \mu \end{aligned} \quad (11)$$

In Fig. 3, we show the amplitude A and frequency ω

of circadian oscillations in perpetual illumination for ten of the eleven models determined using MATLAB ODE solvers [36] scaled by R_s and ω_s into the forms of Eqs. (11). We neglected the model given in Locke *et al.* [4] because the reported parameter set gave two pairs of complex eigenvalues with positive real parts. In the Supplementary Materials, we collapse data from the same ten models in perpetual darkness, and show the collapsed data for each model separately.

For each system, we had to decide which rate parameter to use to define μ , as each system contains more than one parameter whose variation leads to a Hopf bifurcation. To choose which was appropriate, we referenced research that suggests the circadian rhythms in *Arabidopsis* are sensitive to the degradation rates of mRNA [37]. Thus we confined ourselves to using chemical degradation rates as bifurcation parameters.

Of the models we analyzed, the majority employ Michaelis-Menten kinetics [38] to govern the degradation rates of mRNA and protein. A few models use constant degradation rates. We varied the maximum degradation rates in the Michaelis-Menten kinetics or the constant degradation rates one at a time while keeping all other parameters constant. Whenever the variation of one of these parameters led to a Hopf bifurcation, we defined the parameter value at bifurcation as m_c . Motivated by the original work of Stuart [39], we further defined a dimensionless bifurcation parameter,

$$\mu_m = \frac{m_c - m}{m_c} \quad (12)$$

For each model, we investigated the amplitude and frequency scaling (Eqs. (11)) for each μ_m . As each μ_m increased from zero, the scaled quantities deviated from the universal curves. For the purpose of illustration, we present results in Fig. (3) using the bifurcation parameter μ defined to be the μ_m that was largest when the one of the two scaled quantities deviated from the predicted value by ten percent. We note that we did not find a sin-

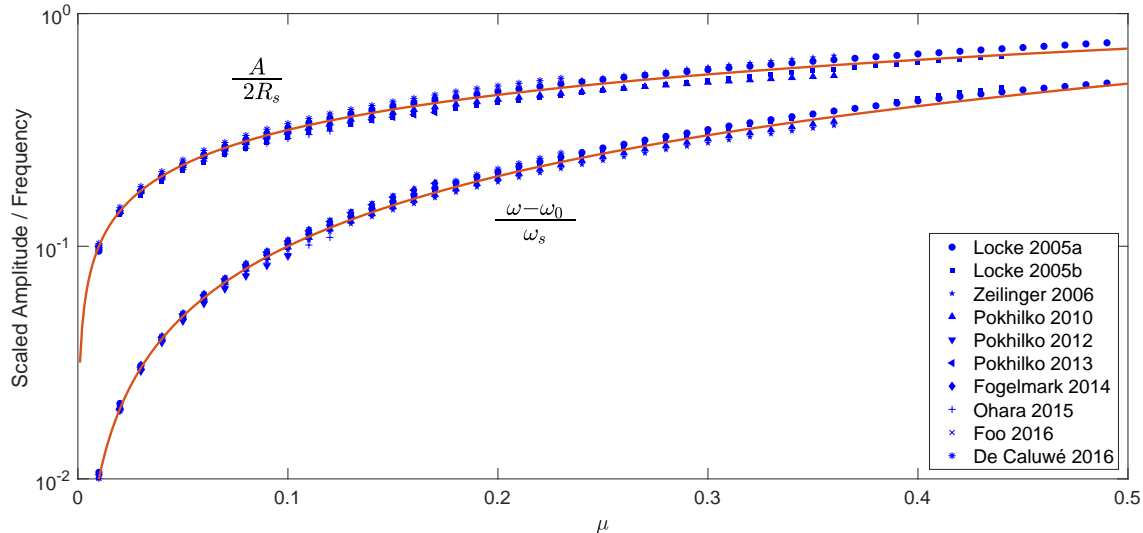


FIG. 3: Amplitude (upper) and frequency (lower) of limit cycle oscillations for ten models of *Arabidopsis* circadian rhythms are collapsed onto universal functions of the bifurcation parameter μ . The limit cycle amplitude and frequency calculated numerically with ODE solvers are scaled with the asymptotic solutions to the Stuart-Landau equation. Data for each model is shown up to the value of μ that they diverge from one of the universal curves by 10%.

gle degradation rate that led to a bifurcation in all the models.

III. DISCUSSION

In this work, we demonstrated that the published dynamical systems models for circadian rhythms in *Arabidopsis thaliana* possess supercritical Hopf bifurcations. We further employed the *Reductive Perturbation Method* (RPM) of Kuramoto [25] to derive an approximate two-dimensional form for the chemical oscillations of the models in the post-bifurcation region of parameter space with a complex amplitude governed by the Stuart-Landau equation. By scaling the amplitude and frequency of the numerical limit cycle solutions with the asymptotic solutions to the Stuart-Landau equation, we showed that all the models possess a common phase space near the Hopf bifurcation.

There are nevertheless significant differences between the models that warrant discussion. Each of the models we investigated contain many rate parameters that were fit to experimental data. The results of these fits vary. Some of the systems we studied are situated on the pre-bifurcation side of a Hopf bifurcation, and others on the post-bifurcation side. Moreover, rate constants that lead to a Hopf bifurcation when varied in some models do not lead to a Hopf bifurcation when varied in other models. We can suggest a possible experimental path to address whether *Arabidopsis* circadian oscillations are post-bifurcation or pre-bifurcation; namely, by driving a plant with a periodic light signal at the free-running fre-

quency over a range of weak intensities. The oscillation amplitude of a pre-bifurcation system should increase linearly with the light intensity while the oscillation amplitude of a post-bifurcation system should not change. In the Supplementary Materials, we show numerical amplitude response curves for both sinusoidal and square-wave forcing.

A second way the models differ is in how close each is to the Hopf bifurcation with their given parameter values, which we measured by comparing the numerical solution to the RPM approximation. The limit cycle amplitude in the model from Locke *et al.* [2] presented in the Methods and Results section matched the RPM calculation to within 0.8% while the limit cycle amplitude from Pokhilko *et al.* [6] shown in Supplementary Materials differed from the RPM calculation by 45.02%. Despite all the differences in the models, including that the genetic network architecture and numerical values of rate constants differed significantly, we showed the dynamical structure of all the models near the bifurcation point is the same. This should be useful in future efforts to fit experimental data close to a supercritical Hopf bifurcation. An experiment that measures a bifurcation curve by varying an external parameter could yield the eigenvalues, eigenvectors, and parameters appearing in Eq. (10). Those quantities could then be used to verify the accuracy of the parameter choices in a particular kinetic model.

Our method of analysis may find application in agricultural engineering projects that use coarse-grained models as valid approximations to weakly nonlinear dynamics to describe an organism-level response to an external stimulus. By using RPM, we are able to arrive at

a coarse-grained form, i.e., the Stuart-Landau equation, as a function of the underlying details of the circadian gene network. The driven Stuart-Landau equation predicts a resonance response of the oscillations that is most pronounced at the Hopf bifurcation point [29]. This resonance behavior near bifurcation suggests a possible engineering program where the chemical kinetics of the organism is tuned, perhaps by varying temperature, to be near the bifurcation point and then driven with a small amplitude (i.e., a low power) sinusoidal light source.

Finally, in recent experiments the circadian oscillations in the cyanobacterium *Synechococcus elongatus* were shown to exhibit a supercritical Hopf bifurcation with temperature as the bifurcation parameter [40]. It has long been noted that commonalities exist in the circadian rhythms of disparate organisms [41]. We tentatively suggest that close proximity to a supercritical Hopf bifurcation may be an additional property favored in the evolutionary development of circadian rhythms. If this suggestion is true, then as we have demonstrated by using the *Reductive Perturbation Method*, circadian rhythms can be cast into

a generic mathematical form given by the Stuart-Landau equation.

ACKNOWLEDGMENTS

The authors would like to thank Harry L. Swinney for a critical reading of the manuscript and helpful conversations. This research was funded by Trinity University with a Murchison Fellowship to Y.X. and start-up funds to O.S.

CODE AVAILABILITY

The MATLAB code to replicate the calculations in this work is available on GitHub at <https://github.com/oshindel/Reductive-Perturbation-Method-A.-thaliana>.

-
- [1] A. J. Millar, The intracellular dynamics of circadian clocks reach for the light of ecology and evolution, *Annual review of plant biology* **67**, 595 (2016).
- [2] J. C. Locke, A. J. Millar, and M. S. Turner, Modelling genetic networks with noisy and varied experimental data: the circadian clock in *arabidopsis thaliana*, *Journal of theoretical biology* **234**, 383 (2005).
- [3] J. C. Locke, M. M. Southern, L. Kozma-Bognár, V. Hibberd, P. E. Brown, M. S. Turner, and A. J. Millar, Extension of a genetic network model by iterative experimentation and mathematical analysis, *Molecular systems biology* **1**, 0013 (2005).
- [4] J. C. Locke, L. Kozma-Bognár, P. D. Gould, B. Fehér, E. Kevei, F. Nagy, M. S. Turner, A. Hall, and A. J. Millar, Experimental validation of a predicted feedback loop in the multi-oscillator clock of *arabidopsis thaliana*, *Molecular systems biology* **2**, 59 (2006).
- [5] M. N. Zeilinger, E. M. Farré, S. R. Taylor, S. A. Kay, and F. J. Doyle, A novel computational model of the circadian clock in *arabidopsis* that incorporates *prp7* and *prp9*, *Molecular Systems Biology* **2**, 58 (2006).
- [6] A. Pokhilko, S. K. Hodge, K. Stratford, K. Knox, K. D. Edwards, A. W. Thomson, T. Mizuno, and A. J. Millar, Data assimilation constrains new connections and components in a complex, eukaryotic circadian clock model, *Molecular systems biology* **6**, 416 (2010).
- [7] A. Pokhilko, A. P. Fernández, K. D. Edwards, M. M. Southern, K. J. Halliday, and A. J. Millar, The clock gene circuit in *arabidopsis* includes a repressilator with additional feedback loops, *Molecular systems biology* **8**, 574 (2012).
- [8] A. Pokhilko, P. Mas, and A. J. Millar, Modelling the widespread effects of *toc1* signalling on the plant circadian clock and its outputs, *BMC systems biology* **7**, 23 (2013).
- [9] K. Fogelmark and C. Troein, Rethinking transcriptional activation in the *arabidopsis* circadian clock, *PLoS computational biology* **10**, e1003705 (2014).
- [10] T. Ohara, H. Fukuda, and I. T. Tokuda, An extended mathematical model for reproducing the phase response of *arabidopsis thaliana* under various light conditions, *Journal of theoretical biology* **382**, 337 (2015).
- [11] M. Foo, D. E. Somers, and P.-J. Kim, Kernel architecture of the genetic circuitry of the *arabidopsis* circadian system, *PLoS computational biology* **12**, e1004748 (2016).
- [12] J. De Caluwé, Q. Xiao, C. Hermans, N. Verbruggen, J.-C. Leloup, and D. Gonze, A compact model for the complex plant circadian clock, *Frontiers in plant science* **7**, 74 (2016).
- [13] N. Bujdoso and S. J. Davis, Mathematical modeling of an oscillating gene circuit to unravel the circadian clock network of *arabidopsis thaliana*, *Frontiers in Plant Science* **4**, 3 (2013).
- [14] Y. H. Chew, R. W. Smith, H. J. Jones, D. D. Seaton, R. Grima, and K. J. Halliday, Mathematical models light up plant signaling, *The Plant Cell* **26**, 5 (2014).
- [15] M. Johansson and T. Köster, On the move through time—a historical review of plant clock research, *Plant Biology* **21**, 13 (2019).
- [16] I. T. Tokuda, O. E. Akman, and J. C. Locke, Reducing the complexity of mathematical models for the plant circadian clock by distributed delays, *Journal of theoretical biology* **463**, 155 (2019).
- [17] M. Foo, D. G. Bates, and O. E. Akman, A simplified modelling framework facilitates more complex representations of plant circadian clocks, *PLoS computational biology* **16**, e1007671 (2020).
- [18] H. Fukuda, N. Nakamichi, M. Hisatsune, H. Murase, and T. Mizuno, Synchronization of plant circadian oscillators with a phase delay effect of the vein network, *Physical Review Letters* **99**, 098102 (2007).

- [19] B. Wenden, D. L. Toner, S. K. Hodge, R. Grima, and A. J. Millar, Spontaneous spatiotemporal waves of gene expression from biological clocks in the leaf, *Proceedings of the National Academy of Sciences* **109**, 6757 (2012).
- [20] H. Fukuda, H. Murase, and I. T. Tokuda, Controlling circadian rhythms by dark-pulse perturbations in *Arabidopsis thaliana*, *Scientific reports* **3**, 1533 (2013).
- [21] M. Endo, H. Shimizu, M. A. Nohales, T. Araki, and S. A. Kay, Tissue-specific clocks in *Arabidopsis* show asymmetric coupling, *Nature* **515**, 419 (2014).
- [22] N. Takahashi, Y. Hirata, K. Aihara, and P. Mas, A hierarchical multi-oscillator network orchestrates the *Arabidopsis* circadian system, *Cell* **163**, 148 (2015).
- [23] M. Endo, Tissue-specific circadian clocks in plants, *Current opinion in plant biology* **29**, 44 (2016).
- [24] P. D. Gould, M. Domijan, M. Greenwood, I. T. Tokuda, H. Rees, L. Kozma-Bognar, A. J. Hall, and J. C. Locke, Coordination of robust single cell rhythms in the *Arabidopsis* circadian clock via spatial waves of gene expression, *Elife* **7**, e31700 (2018).
- [25] Y. Kuramoto, *Chemical oscillations, waves, and turbulence* (Springer-Verlag, Berlin, Heidelberg, 1984).
- [26] M. Anpo, H. Fukuda, and T. Wada, *Plant Factory Using Artificial Light: Adapting to Environmental Disruption and Clues to Agricultural Innovation* (Elsevier, 2018).
- [27] T. Mora and W. Bialek, Are biological systems poised at criticality?, *Journal of Statistical Physics* **144**, 268 (2011).
- [28] M. A. Munoz, Colloquium: Criticality and dynamical scaling in living systems, *Reviews of Modern Physics* **90**, 031001 (2018).
- [29] V. M. Eguíluz, M. Ospeck, Y. Choe, A. Hudspeth, and M. O. Magnasco, Essential nonlinearities in hearing, *Physical review letters* **84**, 5232 (2000).
- [30] A. Hudspeth, F. Jülicher, and P. Martin, A critique of the critical cochlea: Hopf—a bifurcation—is better than none, *Journal of neurophysiology* **104**, 1219 (2010).
- [31] M. Ospeck, V. M. Eguíluz, and M. O. Magnasco, Evidence of a hopf bifurcation in frog hair cells, *Biophysical journal* **80**, 2597 (2001).
- [32] B. D. Hassard, N. D. Kazarinoff, and Y.-H. Wan, *Theory and applications of Hopf bifurcation*, Vol. 41 (CUP Archive, 1981).
- [33] J. Guckenheimer and P. Holmes, Local bifurcations, in *Nonlinear oscillations, dynamical systems, and bifurcations of vector fields* (Springer, 1983) pp. 117–165.
- [34] M. Xiao and J. Cao, Genetic oscillation deduced from hopf bifurcation in a genetic regulatory network with delays, *Mathematical biosciences* **215**, 55 (2008).
- [35] D. Alabadí, T. Oyama, M. J. Yanovsky, F. G. Harmon, P. Más, and S. A. Kay, Reciprocal regulation between *toc1* and *lhy/cca1* within the *Arabidopsis* circadian clock, *Science* **293**, 880 (2001).
- [36] L. F. Shampine and M. W. Reichelt, The matlab ode suite, *SIAM journal on scientific computing* **18**, 1 (1997).
- [37] E. Yakir, D. Hilman, M. Hassidim, and R. M. Green, Circadian clock associated1 transcript stability and the entrainment of the circadian clock in *Arabidopsis*, *Plant physiology* **145**, 925 (2007).
- [38] J. Murray, *Mathematical Biology*, Biomathematics (Springer Berlin Heidelberg, 2013).
- [39] J. T. Stuart, On the non-linear mechanics of hydrodynamic stability, *Journal of Fluid Mechanics* **4**, 1 (1958).
- [40] Y. Murayama, H. Kori, C. Oshima, T. Kondo, H. Iwasaki, and H. Ito, Low temperature nullifies the circadian clock in cyanobacteria through hopf bifurcation, *Proceedings of the National Academy of Sciences* **114**, 5641 (2017).
- [41] C. S. Pittendrigh, Circadian rhythms and the circadian organization of living systems, in *Cold Spring Harbor symposia on quantitative biology*, Vol. 25 (Cold Spring Harbor Laboratory Press, 1960) pp. 159–184.

Universality in Kinetic Models of Circadian Rhythms in *Arabidopsis thaliana*

Yian Xu,^{*} Masoud Asadi-Zeydabadi,[†] Randall Tagg,[†] and Orrin Shindell[‡]
(Dated: September 17, 2021)

SUPPLEMENTARY MATERIALS

Supplementary Tables

In Table S16, we show which models are pre-bifurcation or post-bifurcation with the sets of optimal parameter values reported in the original papers.

In Tables S17 and S18 we show: 1) the kinetic parameter used as the Hopf bifurcation parameter (BP) to produce the data in Fig. 3 of the main text and Figs. S1-S15, 2) the chemical species with the largest modulus used to scale the eigenvectors of the Jacobian matrix at the bifurcation point used to calculate the natural scales, 3) the optimal value of the BP given in the original paper, 4) the critical value of the BP where the Hopf bifurcation occurs, 5) the frequency of zero amplitude oscillations at the bifurcation point, 6) the value of the complex number g in the Stuart-Landau equation, 7) the value of the first order Taylor expansion term, λ_1 , of the eigenvalue of the Jacobian matrix near the bifurcation point.

In Tables S19-S24, we show the several elements of the eigenvectors of the Jacobian matrix at the bifurcation point, normalized by the largest modulus entry, that correspond to LHY and TOC1 protein and *LHY* and *TOC1* mRNA concentrations.

In Table S25, we show which MATLAB ODE solver was used to find the numerical solution for each model and we include comments about our analysis particular to each model.

S1 List of Post-bifurcation and Pre-bifurcation models.

S17 Stuart-Landau parameter values of all models under perpetual illumination.

S18 Stuart-Landau parameter values of all models under perpetual darkness.

S19 Eigenvector entries of the mRNA and proteins of *LHY/CCA1* and *TOC1* genes of Locke et al. 2005a, Locke et al. 2005b, Zeilinger et al. 2006, Pokhilko et al. 2010 models under perpetual illumination.

S20 Eigenvector entries of the mRNA and proteins of *LHY/CCA1* and *TOC1* genes of Pokhilko et al. 2012, Pokhilko et al. 2013, Fogelmark et al. 2014, Ohara et al. 2015 models under perpetual illumination.

S21 Eigenvector entries of the mRNA and proteins of *LHY/CCA1* and *TOC1* genes of Foo et al. 2016 and De Caluwé et al. 2016 models under perpetual illumination.

S22 Eigenvector entries of the mRNA and proteins of *LHY/CCA1* and *TOC1* genes of Locke et al. 2005a, Locke et al. 2005b, Zeilinger et al. 2006, Pokhilko et al. 2010 models under perpetual darkness.

S23 Eigenvector entries of the mRNA and proteins of *LHY/CCA1* and *TOC1* genes of Pokhilko et al. 2012, Pokhilko et al. 2013, Fogelmark et al. 2014, Ohara et al. 2015 models under perpetual darkness.

S24 Eigenvector entries of the mRNA and proteins of *LHY/CCA1* and *TOC1* genes of Foo et al. 2016 and De Caluwé et al. 2016 models under perpetual darkness.

S25 Model idiosyncrasies.

^{*} Trinity University, Physics & Astronomy, San Antonio, Texas, 78212, United States

[†] University of Colorado Denver, Physics, Denver, Colorado, 80203, United States

[‡] oshindel@trinity.edu; Trinity University, Physics & Astronomy, San Antonio, Texas, 78212, United States

Supplementary Figures

In Figs. S1-S12, for all the models we studied whose reported optimal parameters give a post-bifurcation system, we show: 1) bifurcation diagrams for limit cycle amplitude and frequency of *LHY* mRNA, 2) time series for *LHY* mRNA and *TOC1* mRNA limit cycle oscillations, and 3) phase space plots for LHY and TOC1 protein oscillations and *LHY* and *TOC1* mRNA oscillations. Each figure compares the numerical results of the full system of differential equations to the result of the *Reductive Perturbation Method* [1].

In Figs. S14 and S15, we collapse the limit cycle amplitude and frequency of all the models using their respective natural scales. The data is identical to that plotted in Fig. 3 of the main text and Fig. S13, but plotted separately for each model.

S2 Bifurcation diagrams, time series of *LHY* and *TOC1* mRNAs, and phase diagrams for Locke et al. 2005a model under perpetual illumination.

S3 Bifurcation diagrams, time series of *LHY* and *TOC1* mRNAs, and phase diagrams for Locke et al. 2005b model under perpetual illumination.

S4 Bifurcation diagrams, time series of *LHY* and *TOC1* mRNAs, and phase diagrams for Zeilinger et al. 2006 model under perpetual illumination.

S5 Bifurcation diagrams, time series of *LHY* and *TOC1* mRNAs, and phase diagrams for Pokhilko et al. 2010 model under perpetual illumination.

S6 Bifurcation diagrams, time series of *LHY* and *TOC1* mRNAs, and phase diagrams for Pokhilko et al. 2012 model under perpetual illumination.

S7 Bifurcation diagrams, time series of *LHY* and *TOC1* mRNAs, and phase diagrams for Fogelmark et al. 2014 model under perpetual illumination.

S8 Bifurcation diagrams, time series of *LHY* and *TOC1* mRNAs, and phase diagrams for Foo et al. 2016 model under perpetual illumination.

S9 Bifurcation diagrams, time series of *LHY* and *TOC1* mRNAs, and phase diagrams for Locke et al. 2005a model under perpetual darkness.

S10 Bifurcation diagrams, time series of *LHY* and *TOC1* mRNAs, and phase diagrams for Locke et al. 2005b model under perpetual darkness.

S11 Bifurcation diagrams, time series of *LHY* and *TOC1* mRNAs, and phase diagrams for Zeilinger et al. 2006 model under perpetual darkness.

S12 Bifurcation diagrams, time series of *LHY* and *TOC1* mRNAs, and phase diagrams for Foo et al. 2016 model under perpetual darkness.

S13 Bifurcation diagrams, time series of *LHY* and *TOC1* mRNAs, and phase diagrams for De Caluwé et al. 2016 model under perpetual darkness.

S14 Asymptotic amplitude and frequency of oscillation of all models under perpetual darkness.

S15 Asymptotic amplitude and frequency of oscillation of each model under perpetual illumination.

S16 Asymptotic amplitude and frequency of oscillation of each model under perpetual darkness.

Response Curves

We include the derived Stuart-Landau equation with a forcing function and the response curves for both square-wave forcing and sinusoidal forcing. These curves may guide determining whether the system is pre-bifurcation or post-bifurcation from experimental results.

S26 Amplitude response curves for systems that are either pre-bifurcation or post-bifurcation.

List of Pre-bifurcation and Post-Bifurcation Models

Model	Perpetual Illumination	Perpetual Darkness
L2005a	Pre-bifurcation*	Pre-bifurcation*
L2005b	Post-bifurcation	Post-bifurcation
Z2006	Post-bifurcation	Post-bifurcation
P2010	Post-bifurcation	Pre-bifurcation
P2012	Post-bifurcation	Pre-bifurcation
P2013	Pre-bifurcation	Pre-bifurcation
F2014	Post-bifurcation	Pre-bifurcation
O2015	Pre-bifurcation	Pre-bifurcation
F2016	Post-bifurcation	Post-bifurcation
DC2016	Pre-bifurcation	Post-bifurcation

TABLE S16: List indicating which models are pre-bifurcation or post-bifurcation with the sets of optimal parameter values reported in the original papers. Bifurcation diagrams, time series of *LHY* and *TOC1* mRNAs, and the phase diagrams for the post-bifurcation models are shown in Figs. S1-S12.

* The L2005a model is pre-bifurcation with the optimal parameter values but is post-bifurcation with the typical annealed parameter values reported in Fig. 4 of Locke *et al.* [2]. In the Reductive Perturbation Method and the Stuart-Landau Amplitude Equation subsection of the main text we show results using the typical annealed solution, therefore we show the results for L2005a using the typical annealed parameter values in Figs. S2 and S9 and in Tables S17, S18, S19, and S22.

Post-bifurcation Models Results under Perpetual Illumination

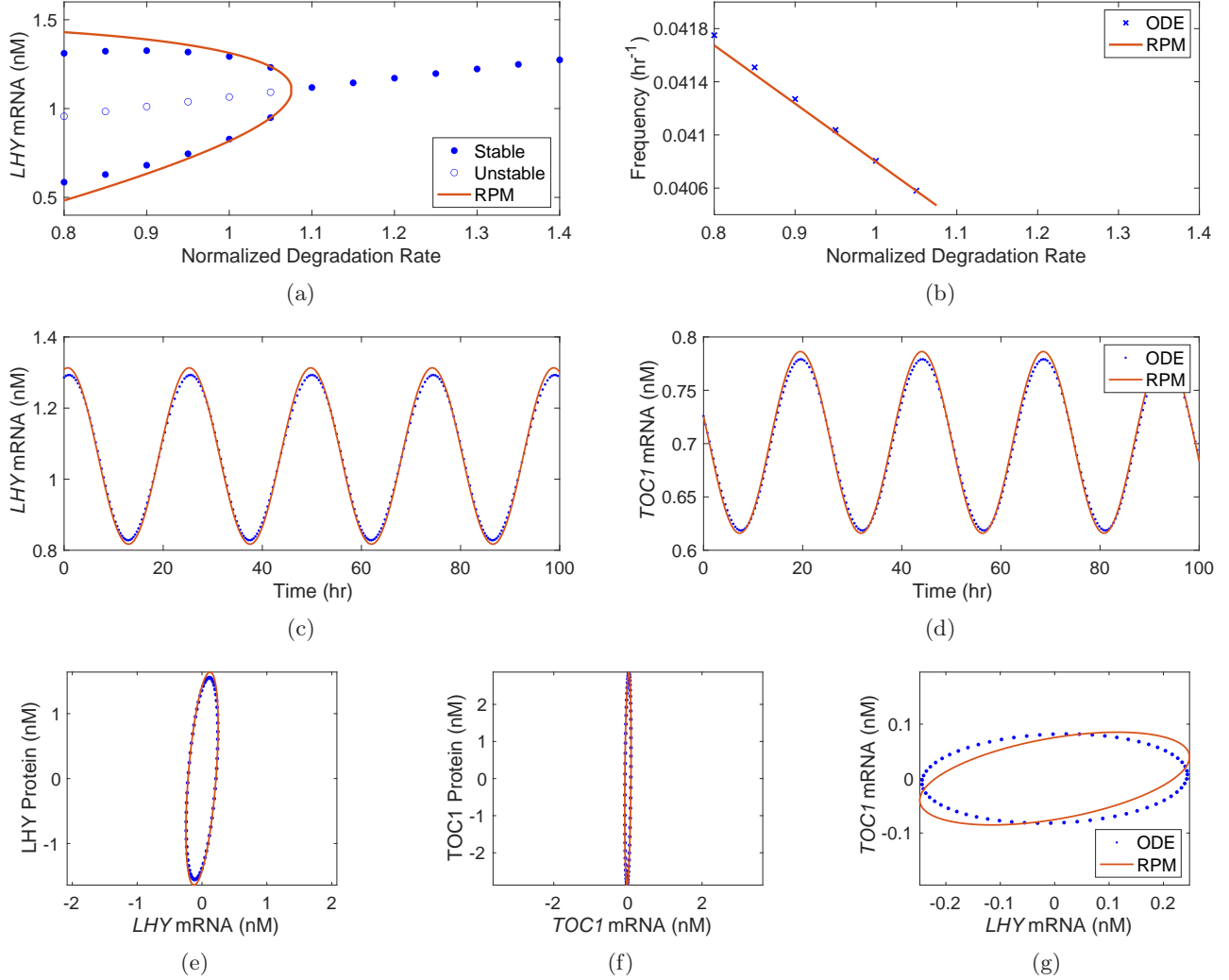


FIG. S1: A supercritical Hopf bifurcation occurs in L2005a model under perpetual illumination. Bifurcation diagrams for (a) concentration of LHY mRNA and (b) frequency of oscillation, time series generated from both ODE and RPM for concentrations of (c) LHY mRNA and (d) $TOC1$ mRNA, and (e) - (g) phase diagrams of pairs of LHY and $TOC1$ protein in the cytoplasm and LHY and $TOC1$ mRNA oscillations are shown. The degradation rate in (a) and (b) are normalized so that the biological value given in the original paper is unity. The amplitude of limit cycle oscillation calculated with RPM matches the numerical solution of the system of ODEs with 6.69 percent difference at biological values; and frequency with 0.006 percent difference. As fractions of 2π , the absolute values of differences in phase difference are 0.006 for the pair (LHY mRNA, LHY protein), 0.001 for the pair ($TOC1$ mRNA, $TOC1$ protein), and 0.063 for the pair (LHY mRNA, $TOC1$ mRNA).

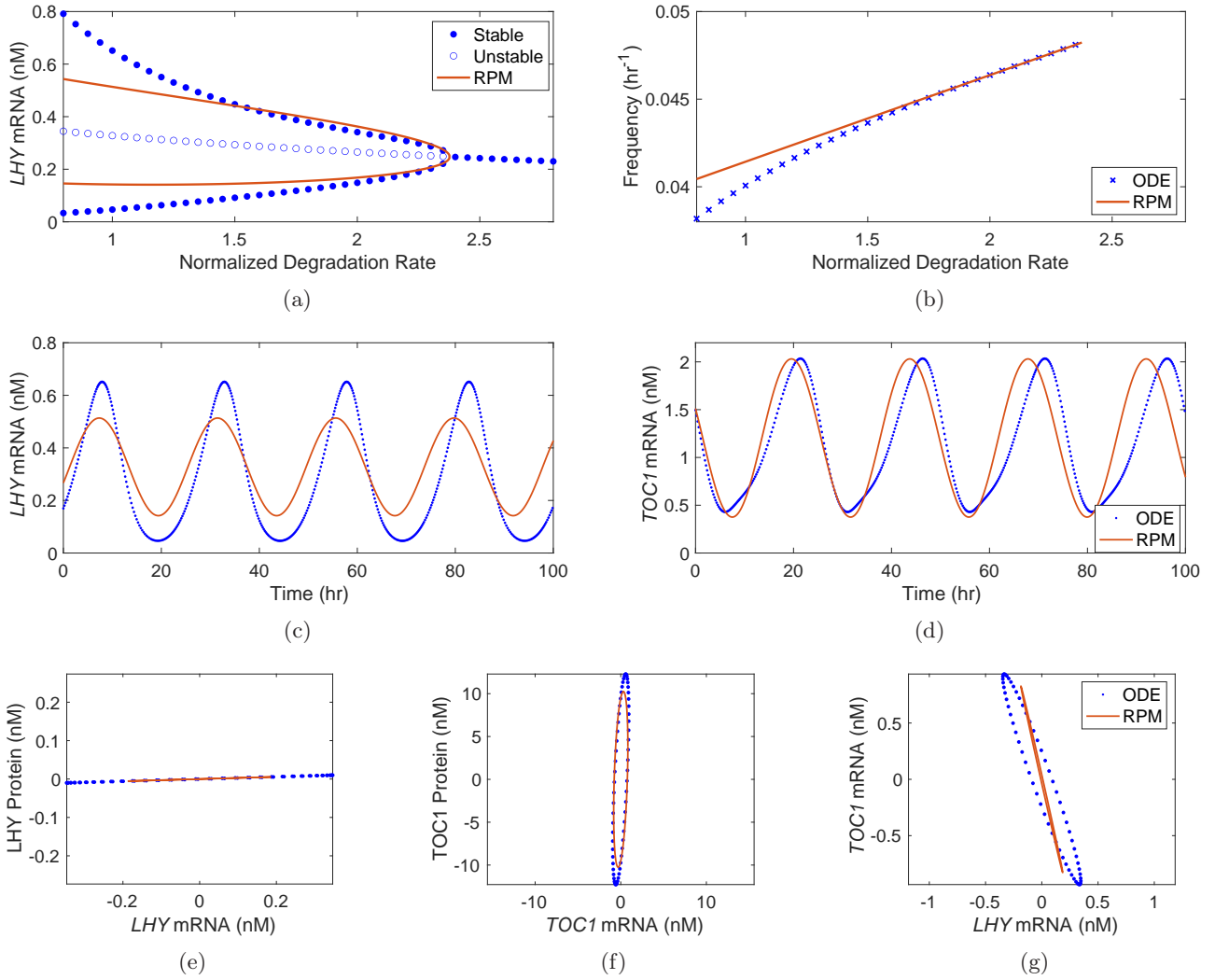


FIG. S2: A supercritical Hopf bifurcation occurs in L2005b model under perpetual illumination. Bifurcation diagrams for (a) concentration of *LHY* mRNA and (b) frequency of oscillation, time series generated from both ODE and RPM for concentrations of (c) *LHY* mRNA and (d) *TOC1* mRNA, and (e) - (g) phase diagrams of pairs of *LHY* and *TOC1* protein in the cytoplasm and *LHY* and *TOC1* mRNA oscillations are shown. The degradation rate in (a) and (b) are normalized so that the biological value given in the original paper is unity. The amplitude of limit cycle oscillation calculated with RPM matches the numerical solution of the system of ODEs with 38.60 percent difference; and frequency with 3.24 percent difference. As fractions of 2π , the absolute values of differences in phase difference are 0.002 for the pair (*LHY* mRNA, *LHY* protein), 0.045 for the pair (*TOC1* mRNA, *TOC1* protein), and 0.035 for the pair (*LHY* mRNA, *TOC1* mRNA).

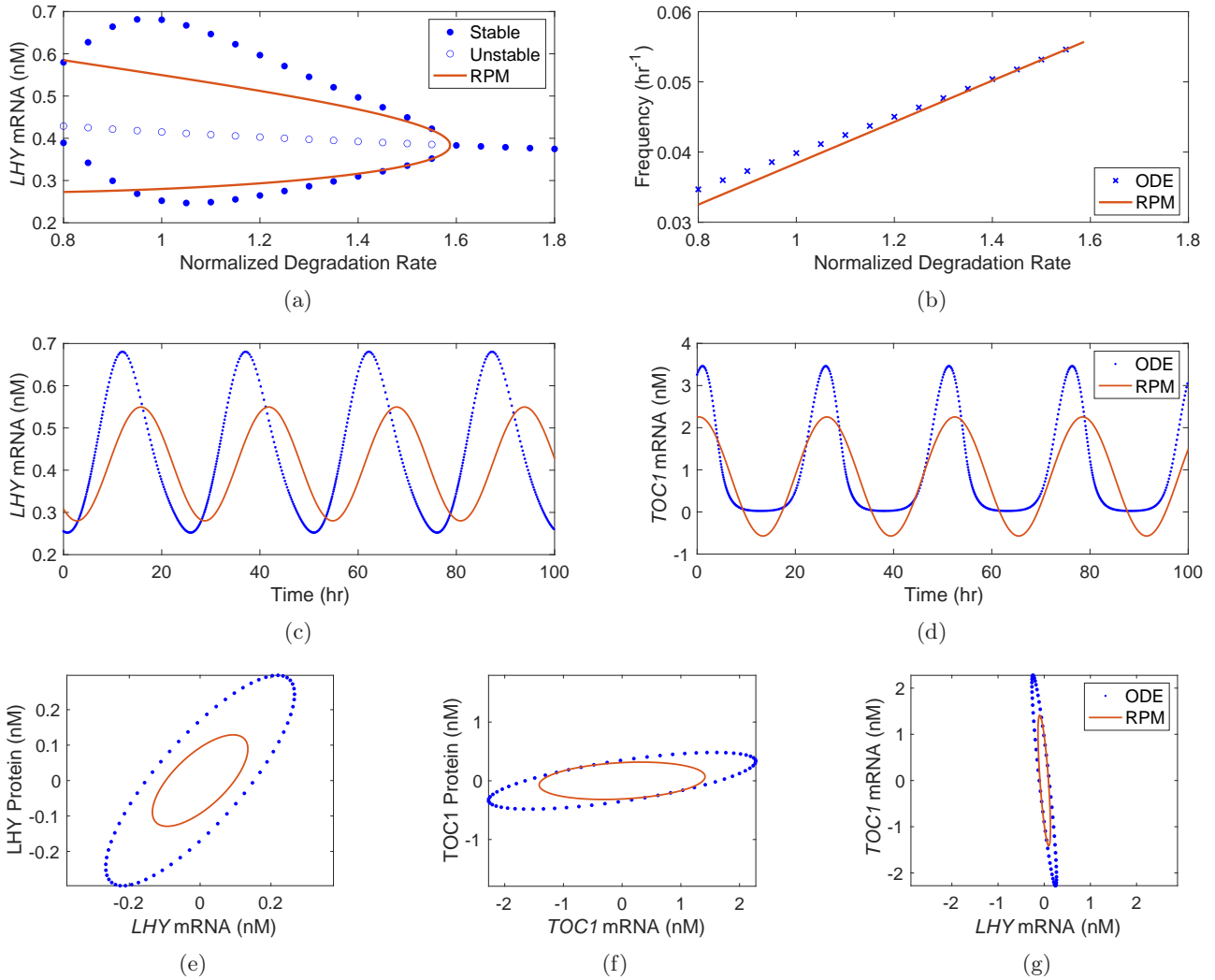


FIG. S3: A supercritical Hopf bifurcation occurs in Z2006 model under perpetual illumination. Bifurcation diagrams for (a) concentration of *LHY* mRNA and (b) frequency of oscillation, time series generated from both ODE and RPM for concentrations of (c) *LHY* mRNA and (d) *TOC1* mRNA, and (e) - (g) phase diagrams of pairs of *LHY* and *TOC1* protein in the cytoplasm and *LHY* and *TOC1* mRNA oscillations are shown. The degradation rate in (a) and (b) are normalized so that the biological value given in the original paper is unity. The amplitude of limit cycle oscillation calculated with RPM matches the numerical solution of the system of ODEs with 37.09 percent difference; and frequency with 3.79 percent difference. As fractions of 2π , the absolute values of differences in phase difference are 0.032 for the pair (*LHY* mRNA, *LHY* protein), 0.085 for the pair (*TOC1* mRNA, *TOC1* protein), and 0.054 for the pair (*LHY* mRNA, *TOC1* mRNA).

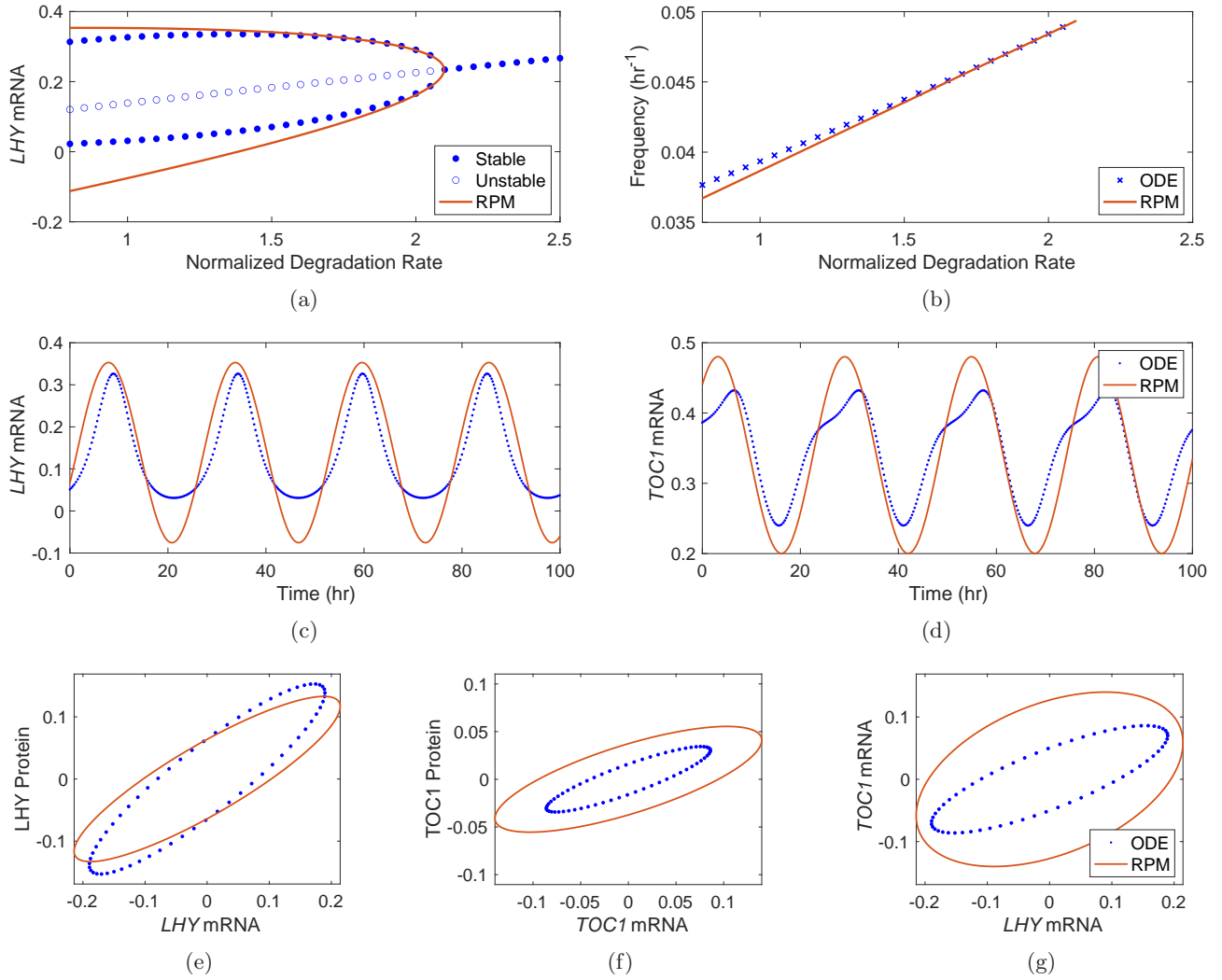


FIG. S4: A supercritical Hopf bifurcation occurs in P2010 model under perpetual illumination. Bifurcation diagrams for (a) concentration of *LHY* mRNA and (b) frequency of oscillation, time series generated from both ODE and RPM for concentrations of (c) *LHY* mRNA and (d) *TOC1* mRNA, and (e) - (g) phase diagrams of pairs of *LHY* and *TOC1* protein in the cytoplasm and *LHY* and *TOC1* mRNA oscillations are shown. The degradation rate in (a) and (b) are normalized so that the biological value given in the original paper is unity. The amplitude of limit cycle oscillation calculated with RPM matches the numerical solution of the system of ODEs with 45.02 percent difference; and frequency with 1.53 percent difference. As fractions of 2π , the absolute values of differences in phase difference are 0.011 for the pair (*LHY* mRNA, *LHY* protein), 0.041 for the pair (*TOC1* mRNA, *TOC1* protein), and 0.082 for the pair (*LHY* mRNA, *TOC1* mRNA).

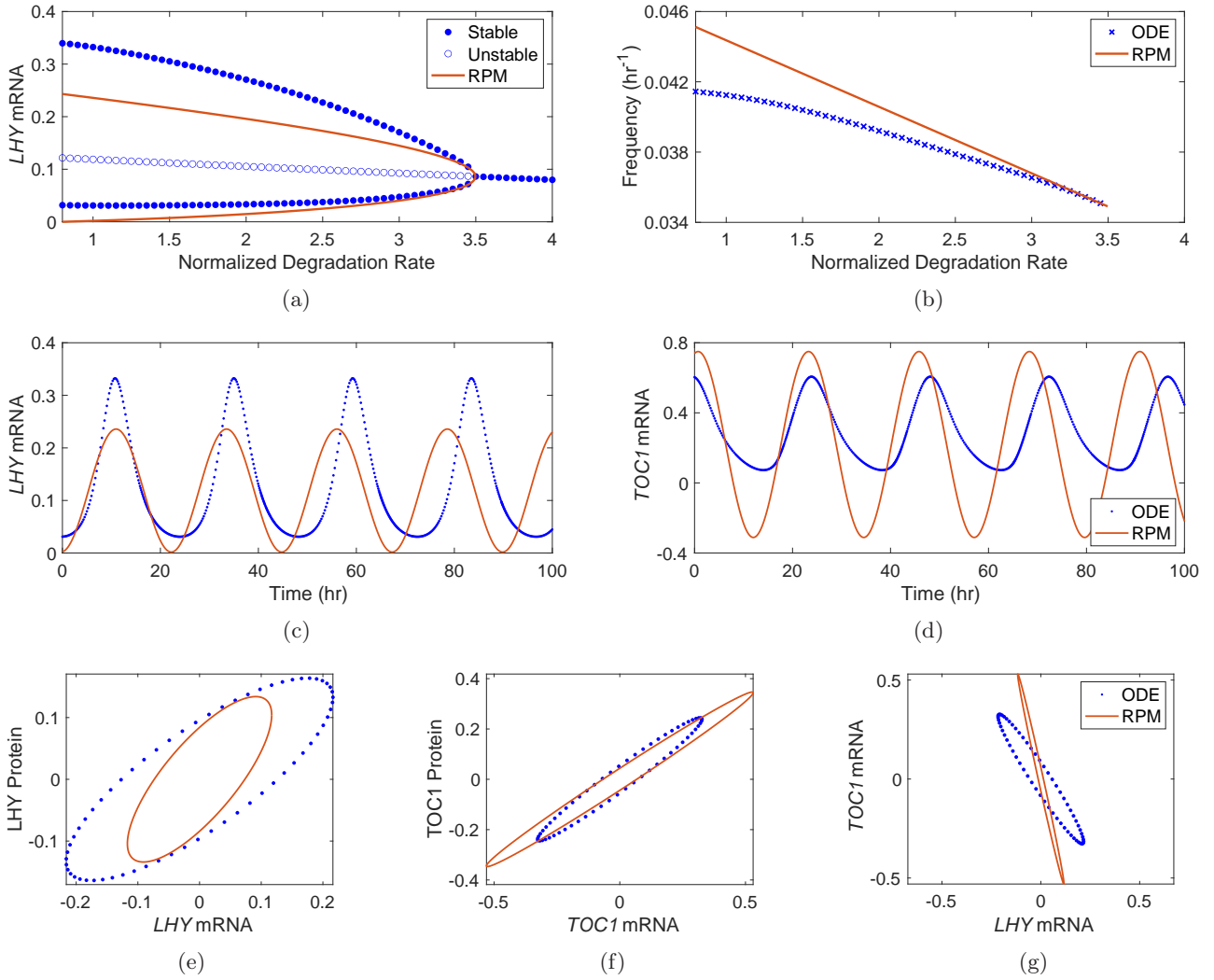


FIG. S5: A supercritical Hopf bifurcation occurs in P2012 model under perpetual illumination. Bifurcation diagrams for (a) concentration of *LHY* mRNA and (b) frequency of oscillation, time series generated from both ODE and RPM for concentrations of (c) *LHY* mRNA and (d) *TOC1* mRNA, and (e) - (g) phase diagrams of pairs of *LHY* and *TOC1* protein in the cytoplasm and *LHY* and *TOC1* mRNA oscillations are shown. The degradation rate in (a) and (b) are normalized so that the biological value given in the original paper is unity. The amplitude of limit cycle oscillation calculated with RPM matches the numerical solution of the system of ODEs with 21.80 percent difference; and frequency with 7.77 percent difference. As fractions of 2π , the absolute values of differences in phase difference are 0.009 for the pair (*LHY* mRNA, *LHY* protein), 0.016 for the pair (*TOC1* mRNA, *TOC1* protein), and 0.024 for the pair (*LHY* mRNA, *TOC1* mRNA).

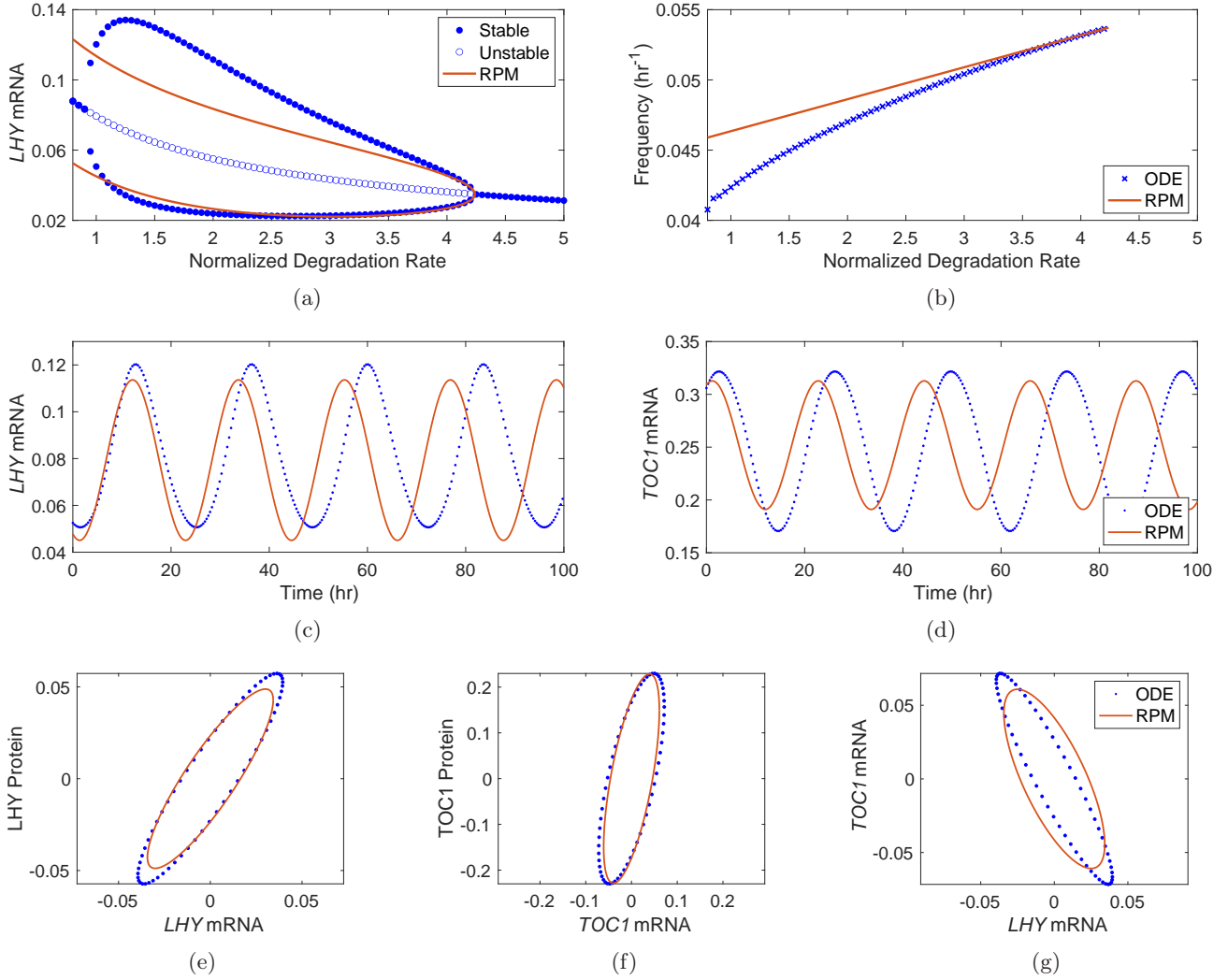


FIG. S6: A supercritical Hopf bifurcation occurs in F2014 model under perpetual illumination. Bifurcation diagrams for (a) concentration of *LHY* mRNA and (b) frequency of oscillation, time series generated from both ODE and RPM for concentrations of (c) *LHY* mRNA and (d) *TOC1* mRNA, and (e) - (g) phase diagrams of pairs of *LHY* and *TOC1* protein in the cytoplasm and *LHY* and *TOC1* mRNA oscillations are shown. The degradation rate in (a) and (b) are normalized so that the biological value given in the original paper is unity. The amplitude of limit cycle oscillation calculated with RPM matches the numerical solution of the system of ODEs with 1.58 percent difference; and frequency with 9.20 percent difference. There is a second Hopf bifurcation near a normalized degradation rate of unity, which is excluded due to our criteria as the pre-bifurcation region for this second bifurcation corresponds to lower degradation rate. As fractions of 2π , the absolute values of differences in phase difference are 0.015 for the pair (*LHY* mRNA, *LHY* protein), 0.006 for the pair (*TOC1* mRNA, *TOC1* protein), and 0.059 for the pair (*LHY* mRNA, *TOC1* mRNA).

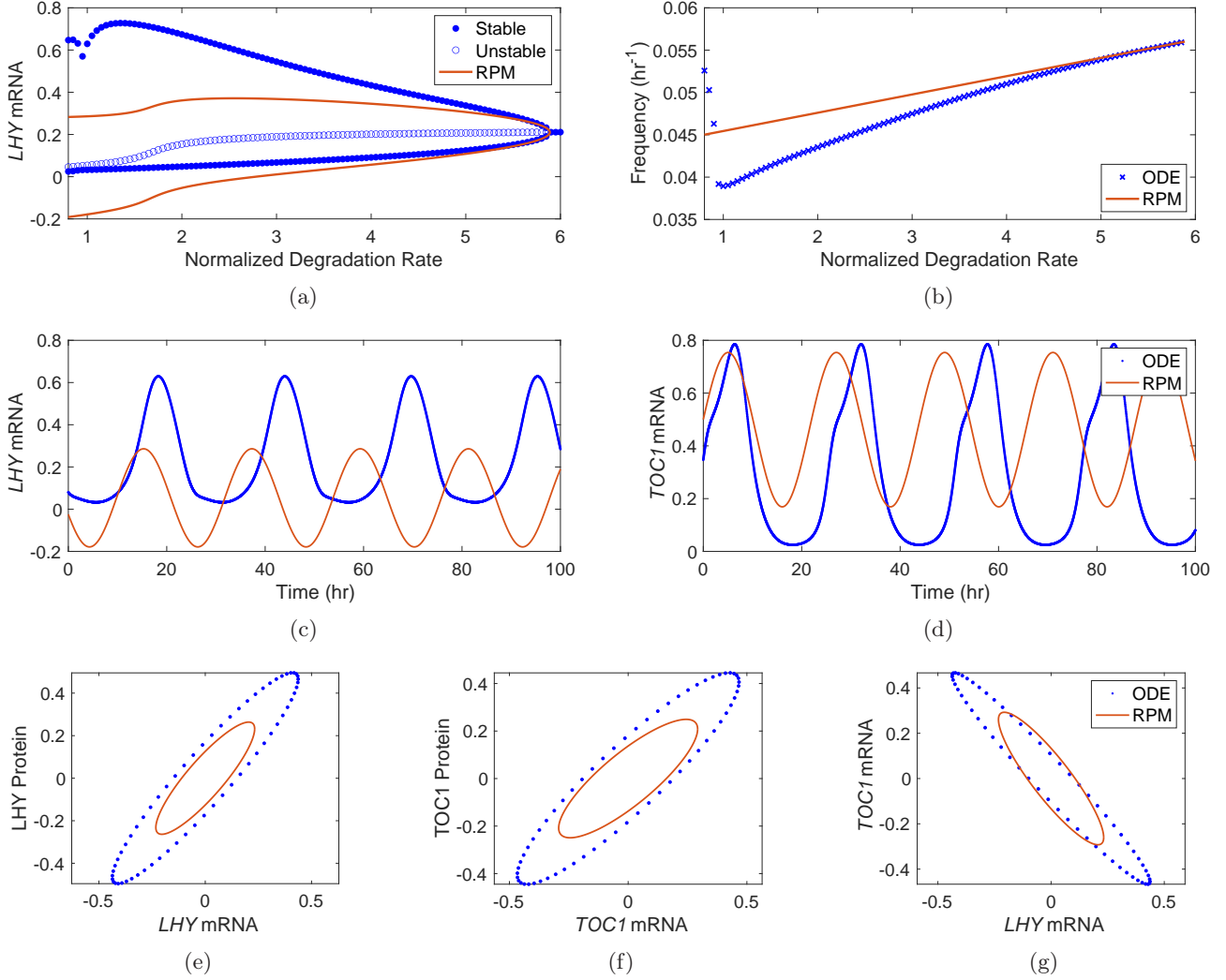


FIG. S7: A supercritical Hopf bifurcation occurs in F2016 model under perpetual illumination. Bifurcation diagrams for (a) concentration of *LHY* mRNA and (b) frequency of oscillation, time series generated from both ODE and RPM for concentrations of (c) *LHY* mRNA and (d) *TOC1* mRNA, and (e) - (g) phase diagrams of pairs of *LHY* and *TOC1* protein in the cytoplasm and *LHY* and *TOC1* mRNA oscillations are shown. The degradation rate in (a) and (b) are normalized so that the biological value given in the original paper is unity. The amplitude of limit cycle oscillation calculated with RPM matches the numerical solution of the system of ODEs with 22.17 percent difference; and frequency with 16.71 percent difference. As fractions of 2π , the absolute values of differences in phase difference are 0.024 for the pair (*LHY* mRNA, *LHY* protein), 0.026 for the pair (*TOC1* mRNA, *TOC1* protein), and 0.039 for the pair (*LHY* mRNA, *TOC1* mRNA).

Post-bifurcation Models Results under Perpetual Darkness

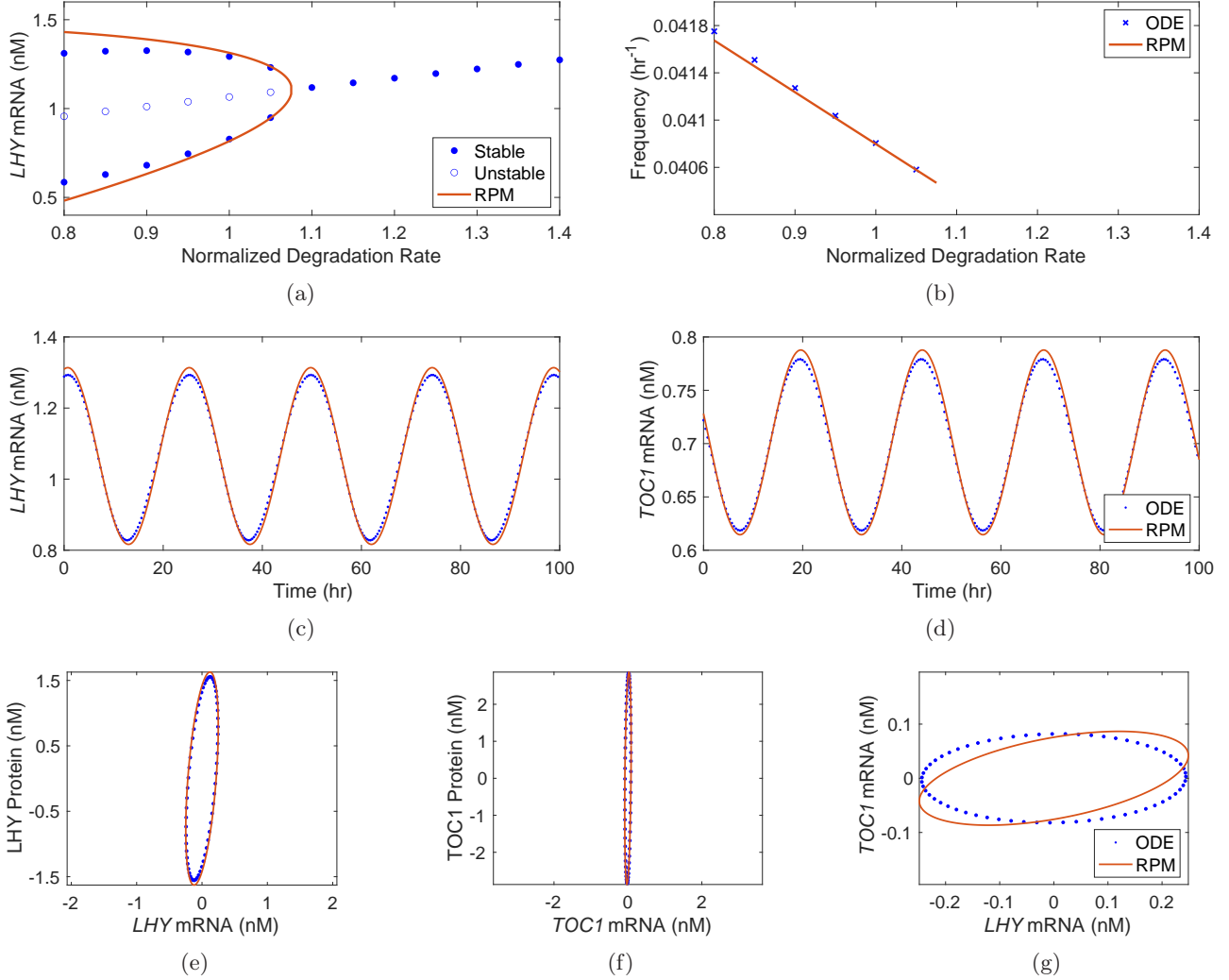


FIG. S8: A supercritical Hopf bifurcation occurs in L2005a model under perpetual darkness. Bifurcation diagrams for (a) concentration of *LHY* mRNA and (b) frequency of oscillation, time series generated from both ODE and RPM for concentrations of (c) *LHY* mRNA and (d) *TOC1* mRNA, and (e) - (g) phase diagrams of pairs of *LHY* and *TOC1* protein in the cytoplasm and *LHY* and *TOC1* mRNA oscillations are shown. The degradation rate in (a) and (b) are normalized so that the biological value given in the original paper is unity. The amplitude of limit cycle oscillation calculated with RPM matches the numerical solution of the system of ODEs with 14.78 percent difference; and frequency with 0.02 percent difference. As fractions of 2π , the absolute values of differences in phase difference are 0.004 for the pair (*LHY* mRNA, *LHY* protein), 0.011 for the pair (*TOC1* mRNA, *TOC1* protein), and 0.074 for the pair (*LHY* mRNA, *TOC1* mRNA).

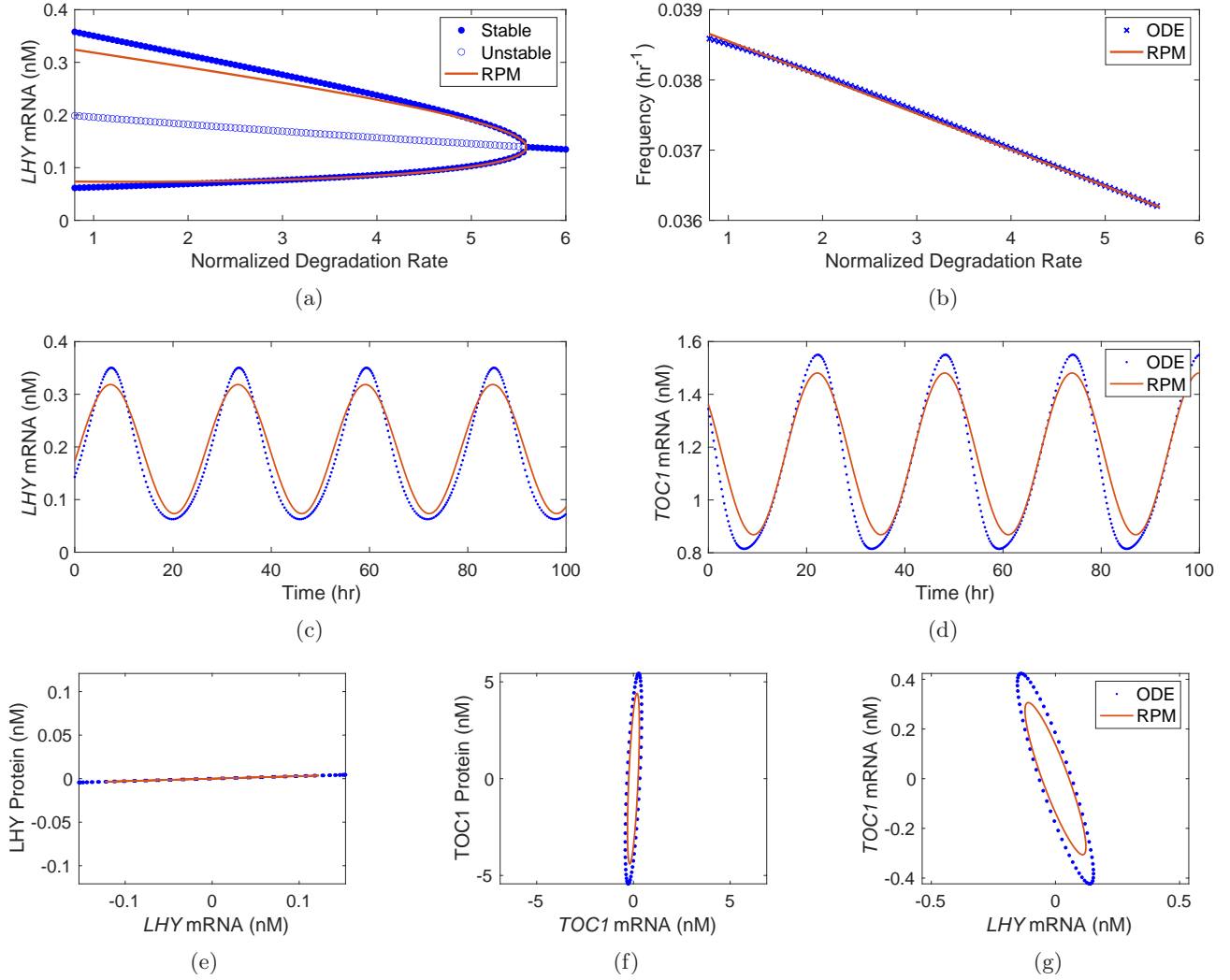


FIG. S9: A supercritical Hopf bifurcation occurs in L2005b model under perpetual darkness. Bifurcation diagrams for (a) concentration of *LHY* mRNA and (b) frequency of oscillation, time series generated from both ODE and RPM for concentrations of (c) *LHY* mRNA and (d) *TOC1* mRNA, and (e) - (g) phase diagrams of pairs of *LHY* and *TOC1* protein in the cytoplasm and *LHY* and *TOC1* mRNA oscillations are shown. The degradation rate in (a) and (b) are normalized so that the biological value given in the original paper is unity. The amplitude of limit cycle oscillation calculated with RPM matches the numerical solution of the system of ODEs with 14.78 percent difference; and frequency with 0.26 percent difference. As fractions of 2π , the absolute values of differences in phase difference are 0.0003 for the pair (*LHY* mRNA, *LHY* protein), 0.004 for the pair (*TOC1* mRNA, *TOC1* protein), and 0.003 for the pair (*LHY* mRNA, *TOC1* mRNA).

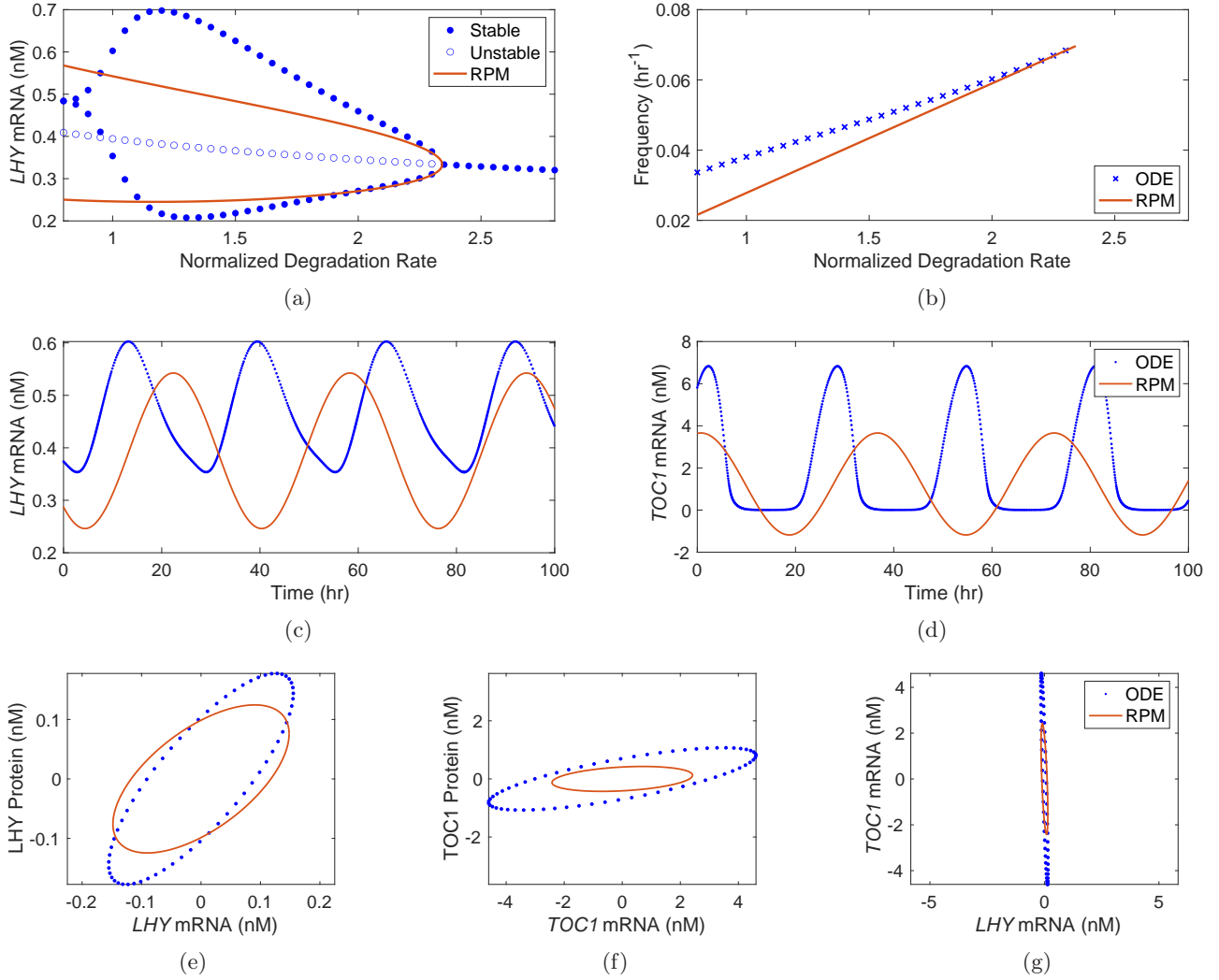


FIG. S10: A supercritical Hopf bifurcation occurs in Z2006 model under perpetual darkness. Bifurcation diagrams for (a) concentration of *LHY* mRNA and (b) frequency of oscillation, time series generated from both ODE and RPM for concentrations of (c) *LHY* mRNA and (d) *TOC1* mRNA, and (e) - (g) phase diagrams of pairs of *LHY* and *TOC1* protein in the cytoplasm and *LHY* and *TOC1* mRNA oscillations are shown. The degradation rate in (a) and (b) are normalized so that the biological value given in the original paper is unity. The amplitude of limit cycle oscillation calculated with RPM matches the numerical solution of the system of ODEs with 19.04 percent difference; and frequency with 27.03 percent difference. As fractions of 2π , the absolute values of differences in phase difference are 0.046 for the pair (*LHY* mRNA, *LHY* protein), 0.089 for the pair (*TOC1* mRNA, *TOC1* protein), and 0.058 for the pair (*LHY* mRNA, *TOC1* mRNA).

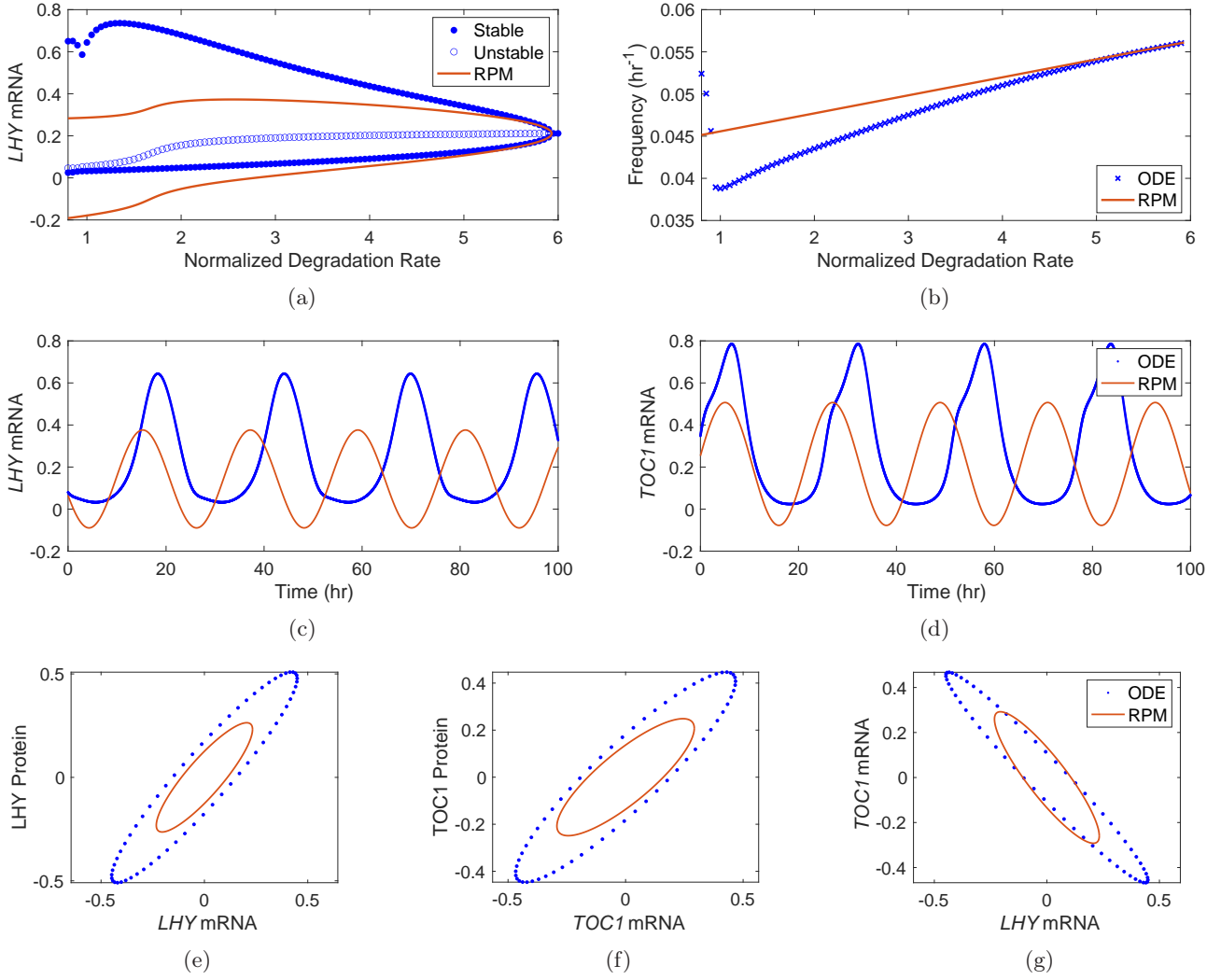


FIG. S11: A supercritical Hopf bifurcation occurs in F2016 model under perpetual darkness. Bifurcation diagrams for (a) concentration of *LHY* mRNA and (b) frequency of oscillation, time series generated from both ODE and RPM for concentrations of (c) *LHY* mRNA and (d) *TOC1* mRNA, and (e) - (g) phase diagrams of pairs of *LHY* and *TOC1* protein in the cytoplasm and *LHY* and *TOC1* mRNA oscillations are shown. The degradation rate in (a) and (b) are normalized so that the biological value given in the original paper is unity. The amplitude of limit cycle oscillation calculated with RPM matches the numerical solution of the system of ODEs with 23.88 percent difference; and frequency with 17.53 percent difference. As fractions of 2π , the absolute values of differences in phase difference are 0.024 for the pair (*LHY* mRNA, *LHY* protein), 0.026 for the pair (*TOC1* mRNA, *TOC1* protein), and 0.039 for the pair (*LHY* mRNA, *TOC1* mRNA).

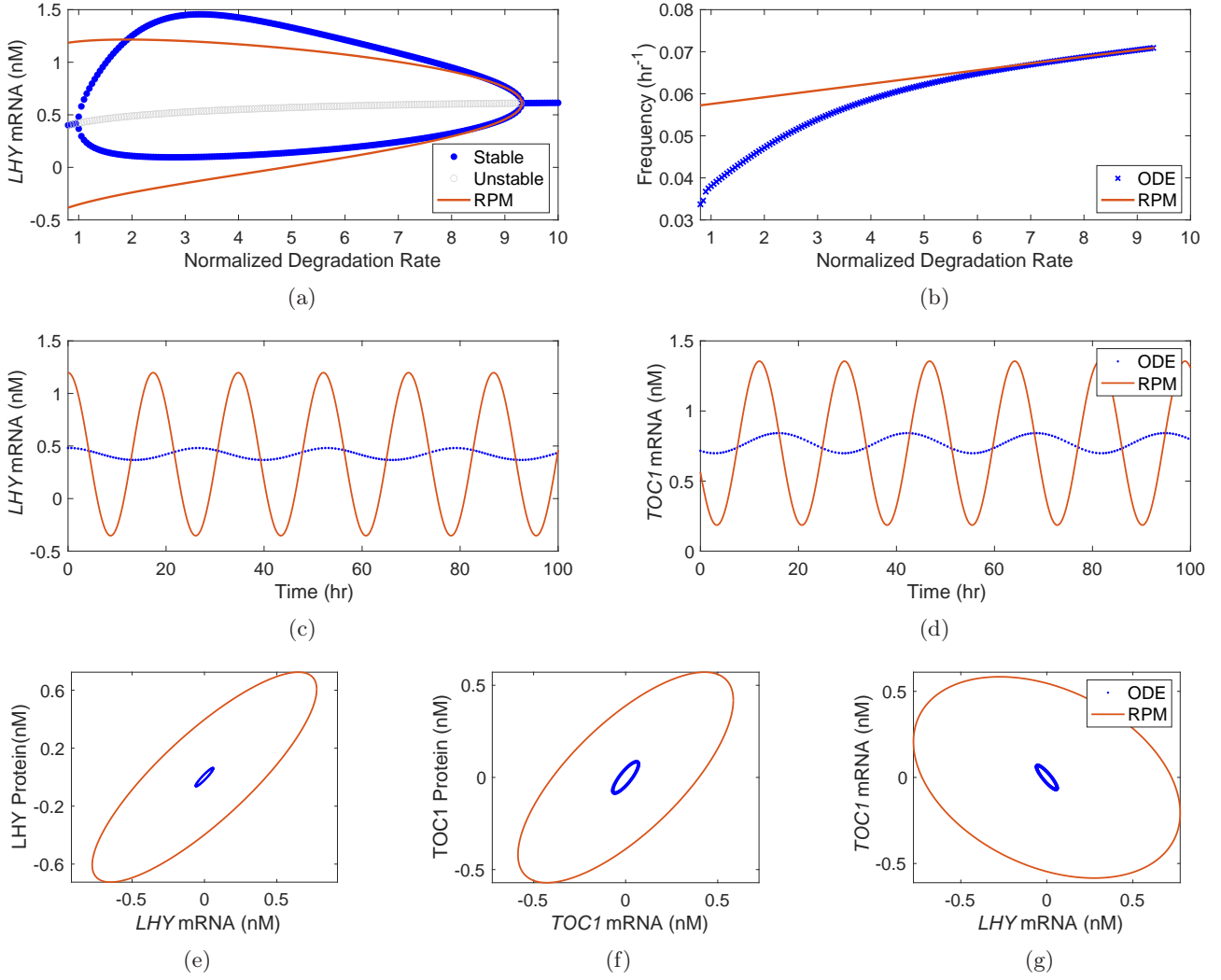


FIG. S12: A supercritical Hopf bifurcation occurs in DC2016 model under perpetual darkness. Bifurcation diagrams for (a) concentration of *LHY* mRNA and (b) frequency of oscillation, time series generated from both ODE and RPM for concentrations of (c) *LHY* mRNA and (d) *TOC1* mRNA, and (e) - (g) phase diagrams of pairs of *LHY* and *TOC1* protein in the cytoplasm and *LHY* and *TOC1* mRNA oscillations are shown. The degradation rate in (a) and (b) are normalized so that the biological value given in the original paper is unity. The amplitude of limit cycle oscillation calculated with RPM matches the numerical solution of the system of ODEs with 1267.28 percent difference; and frequency with 51.58 percent difference. There is a second Hopf bifurcation near a normalized degradation rate of unity, which is excluded due to our criteria as the pre-bifurcation region for this second bifurcation corresponds to lower degradation rate. As fractions of 2π , the absolute values of differences in phase difference are 0.039 for the pair (*LHY* mRNA, *LHY* protein), 0.027 for the pair (*TOC1* mRNA, *TOC1* protein), and 0.113 for the pair (*LHY* mRNA, *TOC1* mRNA).

Asymptotic amplitude and frequency of oscillation for all models under Perpetual Darkness

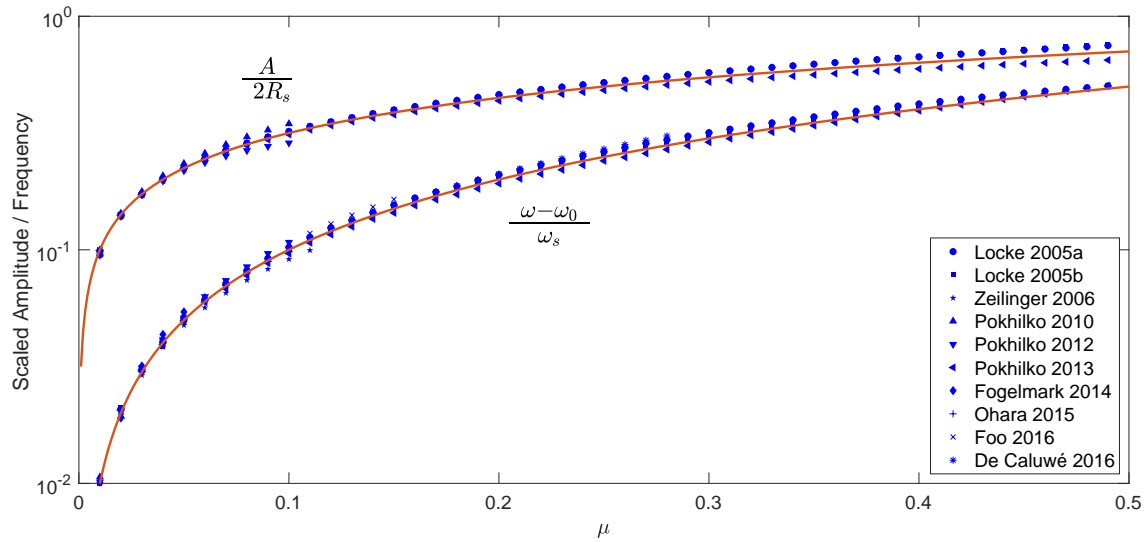


FIG. S13: Amplitude and frequency of limit cycle oscillations for ten models of *Arabidopsis* circadian rhythms in perpetual darkness collapsed onto universal functions of the bifurcation parameter μ . The limit cycle amplitude and frequency calculated numerically with ODE solvers are scaled with the asymptotic solutions to the Stuart-Landau equation. Data for each model is shown up to the value of μ that they diverge from one of the universal curves by 10%.

Asymptotic amplitude and frequency of oscillation for each model under Perpetual Illumination

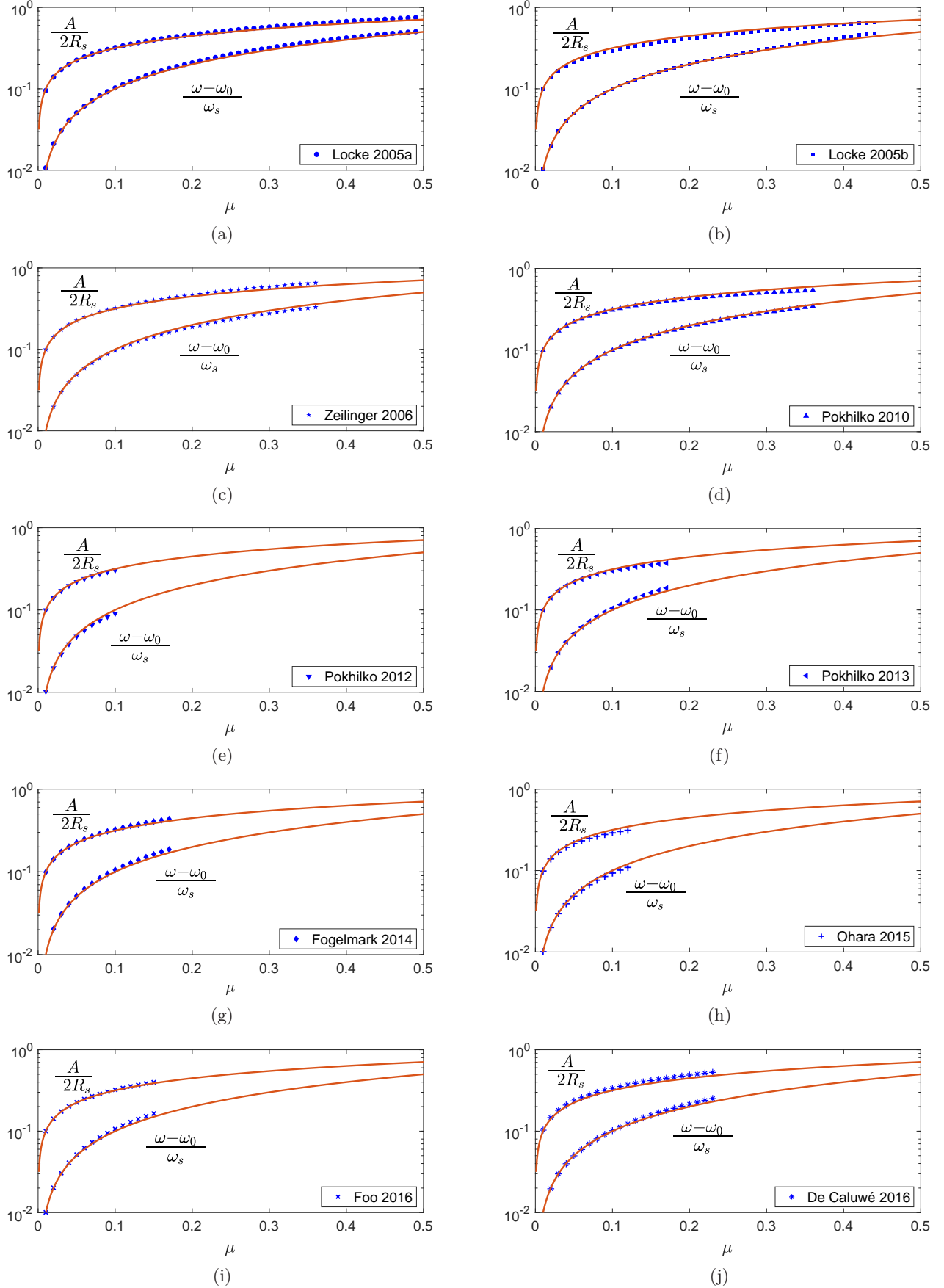
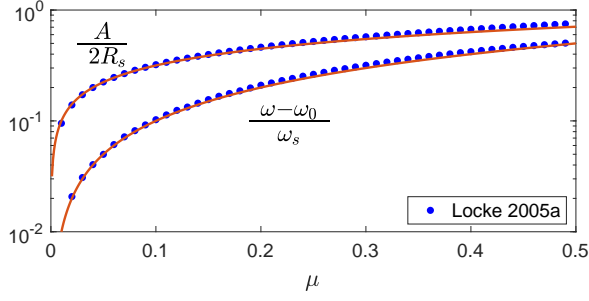
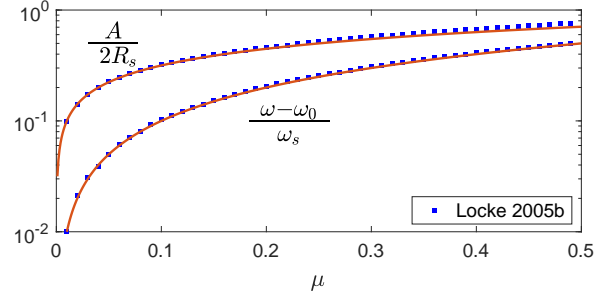


FIG. S14: Amplitude and frequency collapse for each model under perpetual illumination.

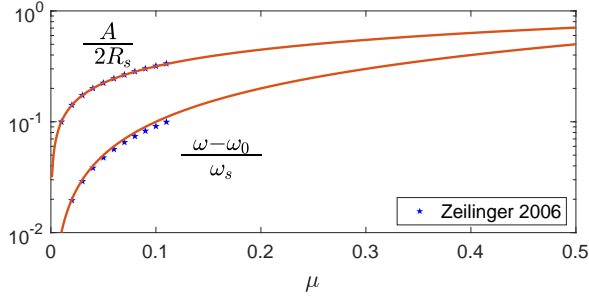
Asymptotic amplitude and frequency of oscillation for each model under Perpetual Darkness



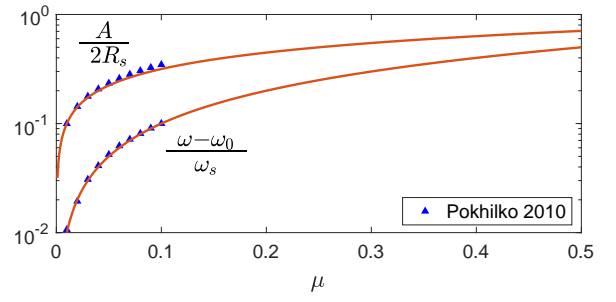
(a)



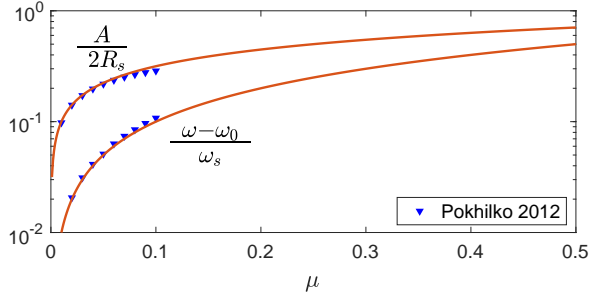
(b)



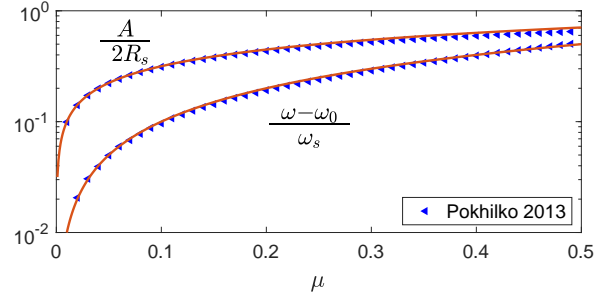
(c)



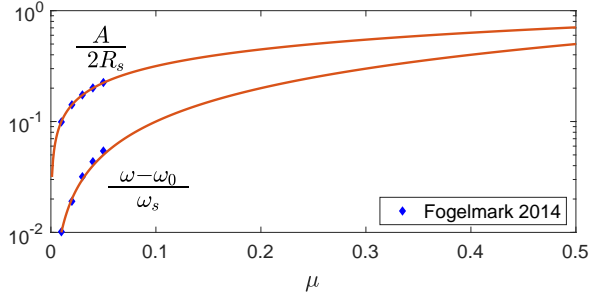
(d)



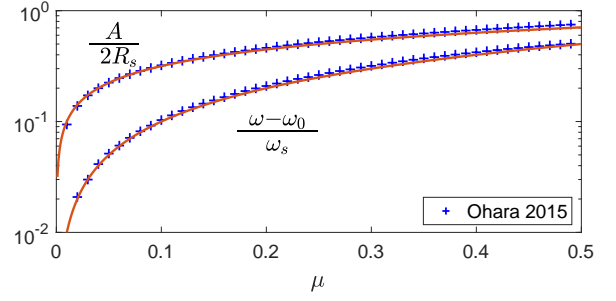
(e)



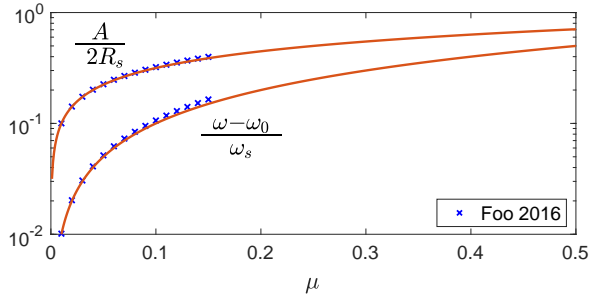
(f)



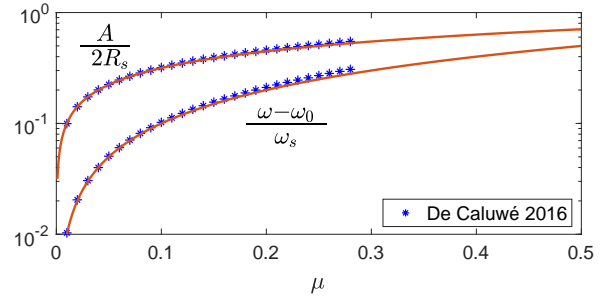
(g)



(h)



(i)



(j)

FIG. S15: Amplitude and frequency collapse for each model under perpetual darkness.

Stuart-Landau Parameter Values under Perpetual Illumination

Model	BP	Scaled By	Optimal Value	Critical Value
L2005a	m_2	TOC1 _c	16.9058	6.2609
L2005b	m_1	TOC1 _c	1.5283	3.6327
Z2006	m_{12}	Y _n	5.9504	9.4460
P2010	m_3	Y Protein	0.2	0.4195
P2012	m_{35}	LUX	0.3	1.0493
P2013	m_{15}	LUX	0.7	0.4099
F2014	m_1	PPR7 mRNA	0.6127	2.5971
O2015	m_1	TOC1 _c	9.3383	9.0593
F2016	ϕ_{36}	PPR7 mRNA	0.37854	2.2289
DC2016	d_7	ELF4/LUX Protein	0.38	0.2232

Model	ω_0	$g = g' + ig''$	$\lambda_1 = \sigma_1 + i\omega_1$
L2005a	0.3013	0.1686 + 0.1471 <i>i</i>	0.0022 + 0.0088 <i>i</i>
L2005b	0.3031	0.0003 + 0.0000 <i>i</i>	0.0041 - 0.0197 <i>i</i>
Z2006	0.3500	0.0015 + 0.0070 <i>i</i>	0.0054 - 0.0059 <i>i</i>
P2010	0.3101	0.1844 + 0.4475 <i>i</i>	0.0929 - 0.0807 <i>i</i>
P2012	0.2193	0.0573 + 0.0056 <i>i</i>	0.0656 + 0.0857 <i>i</i>
P2013	0.2647	0.0472 + 0.0595 <i>i</i>	0.0382 - 0.0269 <i>i</i>
F2014	0.3375	0.1259 + 0.0817 <i>i</i>	0.0131 - 0.0149 <i>i</i>
O2015	0.2614	0.1076 + 0.0817 <i>i</i>	0.0099 + 0.0206 <i>i</i>
F2016	0.3519	0.7441 + 0.3900 <i>i</i>	0.0215 - 0.0246 <i>i</i>
DC2016	0.2477	0.1318 + 0.1077 <i>i</i>	0.0979 - 0.2052 <i>i</i>

TABLE S17: Bifurcation parameters (BP), the chemical species that corresponds to the component in the eigenvectors with the largest modulus (Scaled By), optimal and critical values of the bifurcation parameter for each model, along with important Stuart-Landau parameters. Calculations and simulations are conducted under perpetual illumination.

Stuart-Landau Parameter Values under Perpetual Darkness

Model	BP	Scaled By	Optimal Value	Critical Value
L2005a	m_2	TOC1 _c	16.9058	6.2609
L2005b	m_{13}	TOC1 _c	0.1347	0.7518
Z2006	m_{12}	Y _n	5.9504	13.9347
P2010	m_{10}	Y Protein	0.3	0.2751
P2012	m_{19}	LUX	0.2	0.0738
P2013	m_{15}	LUX	0.7	0.6589
F2014	m_{31}	LUX	0.3	0.1017
O2015	m_2	TOC1 _c	16.9058	6.2609
F2016	ϕ_{36}	<i>PPR7</i> mRNA	0.37854	2.2453
DC2016	k_2	<i>CCA1/LHY</i> mRNA	0.21	1.9574

Model	ω_0	$g = g' + ig''$	$\lambda_1 = \sigma_1 + i\omega_1$
L2005a	0.3013	0.1686 + 0.1471 <i>i</i>	0.0022 + 0.0088 <i>i</i>
L2005b	0.2274	0.0030 - 0.0010 <i>i</i>	0.0232 + 0.0160 <i>i</i>
Z2006	0.4377	0.0015 + 0.0086 <i>i</i>	0.0050 - 0.0035 <i>i</i>
P2010	0.1952	1.0472 + 0.2216 <i>i</i>	0.1800 + 0.1757 <i>i</i>
P2012	0.2225	0.0691 + 0.0539 <i>i</i>	0.1013 - 0.5555 <i>i</i>
P2013	0.2541	0.0655 + 0.0725 <i>i</i>	0.0245 + 0.0171 <i>i</i>
F2014	0.2842	0.0343 + 0.0411 <i>i</i>	0.1516 + 0.2601 <i>i</i>
O2015	0.3013	0.1686 + 0.1471 <i>i</i>	0.0022 + 0.0088 <i>i</i>
F2016	0.3523	0.7458 + 0.3953 <i>i</i>	0.0213 - 0.0242 <i>i</i>
DC2016	0.4457	0.5415 + 0.6186 <i>i</i>	0.0466 + 0.0051 <i>i</i>

TABLE S18: Bifurcation parameters (BP), the chemical species that corresponds to the component in the eigenvectors with the largest modulus (Scaled By), optimal and critical values of the bifurcation parameter for each model, along with important Stuart-Landau parameters. Calculations and simulations are conducted under perpetual darkness.

Eigenvector Entries under Perpetual Illumination

Chemical Species	L2005a	L2005b
<i>LHY</i> mRNA	-0.0065 - 0.1770i	-0.0060 - 0.0171i
LHY protein cytoplasm	-0.0406 - 0.2550i	-0.0002 - 0.0005i
LHY protein nucleus	-0.0658 - 0.1958i	-0.0013 - 0.0027i
<i>TOC1</i> mRNA	0.1283 + 0.2329i	0.0302 + 0.0749i
TOC1 protein cytoplasm	1.0000 + 0.0000i	1.0000 + 0.0000i
TOC1 protein nucleus	0.0088 - 0.1492i	0.0998 - 0.0096i

Chemical Species	Z2006	P2010
<i>LHY</i> mRNA	-0.0150 + 0.0116i	-0.1086 - 0.3031i
LHY protein cytoplasm	-0.0019 + 0.0180i	-0.1496 - 0.1325i
LHY protein nucleus	-0.0009 + 0.0090i	-0.0759 + 0.0213i
<i>TOC1</i> mRNA	0.1978 - 0.0181i	0.1504 - 0.1471i
TOC1 protein cytoplasm	0.0060 - 0.0443i	0.0048 - 0.0832i
TOC1 protein nucleus	0.0241 - 0.2542i	-0.0196 - 0.0198i

TABLE S19: Eigenvector entries for the mRNA and proteins of *LHY/CCA1* and *TOC1* genes under perpetual illumination. For P2010 model, the second and fifth entries are protein (LHY and TOC1 in Pokhilko et al. 2010), and the third and sixth entries are modified protein (LHY_{mod} and $TOC1_{\text{mod}}$ in Pokhilko et al. 2010).

Chemical Species	P2012	P2013
<i>LHY</i> mRNA	-0.0629 - 0.0056i	-0.0999 - 0.1054i
LHY protein cytoplasm	-0.0601 + 0.0402i	-0.1464 - 0.0116i
LHY protein nucleus	-0.0026 + 0.0173i	-0.0275 + 0.0310i
<i>TOC1</i> mRNA	0.2803 - 0.0578i	0.1630 + 0.0013i
TOC1 protein cytoplasm	0.1770 - 0.0606i	0.0938 - 0.0310i
TOC1 protein nucleus		

Chemical Species	F20014	O2015
<i>LHY</i> mRNA	-0.0347 + 0.0147i	-0.0479 - 0.3371i
LHY protein cytoplasm	-0.0333 + 0.0422i	-0.0392 - 0.2089i
LHY protein nucleus		-0.0530 - 0.1568i
<i>TOC1</i> mRNA	0.0630 - 0.0229i	0.1083 + 0.2022i
TOC1 protein cytoplasm	0.0887 - 0.2355i	1.0000 + 0.0000i
TOC1 protein nucleus	0.0127 - 0.0313i	0.0061 - 0.1723i

TABLE S20: Eigenvector entries for the mRNA and proteins of *LHY/CCA1* and *TOC1* genes under perpetual illumination continued. Empty entries are due to different definitions of variables.

Chemical Species	F2016	DC2016
<i>LHY</i> mRNA	-0.1688 + 0.4729i	-0.0813 - 0.3151i
LHY protein	0.0881 + 0.5630i	-0.3003 - 0.4373i
<i>TOC1</i> mRNA	0.0831 - 0.6266i	0.6043 + 0.4132i
TOC1 protein	-0.3526 - 0.4070i	0.5482 + 0.1650i

TABLE S21: Eigenvector entries for the mRNA and proteins of *LHY/CCA1* and *TOC1* genes under perpetual illumination continued. F2016 and DC2016 models use only one variable for proteins of *LHY* and *TOC1*. The *TOC1* entries represent *PRR5/TOC1* gene group.

Eigenvector Entries under Perpetual Darkness

Chemical Species	L2005a	L2005b
<i>LHY</i> mRNA	-0.0065 - 0.1770i	-0.0054 - 0.0273i
LHY protein cytoplasm	-0.0406 - 0.2550i	-0.0002 - 0.0008i
LHY protein nucleus	-0.0658 - 0.1958i	-0.0013 - 0.0044i
<i>TOC1</i> mRNA	0.1283 + 0.2329i	0.0426 + 0.0550i
TOC1 protein cytoplasm	1.0000 + 0.0000i	1.0000 + 0.0000i
TOC1 protein nucleus	0.0088 - 0.1492i	0.0815 - 0.0048i

Chemical Species	Z2006	P2010
<i>LHY</i> mRNA	-0.0102 + 0.0098i	-0.5879 - 0.2651i
LHY protein cytoplasm	0.0013 + 0.0118i	-0.4563 + 0.0538i
LHY protein nucleus	0.0007 + 0.0059i	-0.1291 + 0.1596i
<i>TOC1</i> mRNA	0.2296 - 0.0305i	0.2702 - 0.1906i
TOC1 protein cytoplasm	0.0067 - 0.0405i	0.0825 - 0.2191i
TOC1 protein nucleus	0.0270 - 0.2324i	-0.0712 - 0.1066i

TABLE S22: Eigenvector entries for the mRNA and proteins of *LHY/CCA1* and *TOC1* genes under perpetual darkness. For P2010 model, the second and fifth entries are protein (LHY and TOC1 in Pokhilko et al. 2010), and the third and sixth entries are modified protein (LHY_{mod} and TOC1_{mod} in Pokhilko et al. 2010).

Chemical Species	P2012	P2013
<i>LHY</i> mRNA	-0.2115 - 0.1598i	-0.0851 - 0.1892i
LHY protein cytoplasm	-0.1884 - 0.0041i	-0.1261 - 0.0620i
LHY protein nucleus	-0.0466 + 0.0496i	-0.0420 + 0.0201i
<i>TOC1</i> mRNA	0.1737 + 0.0253i	0.0827 + 0.0256i
TOC1 protein cytoplasm	0.0727 - 0.0015i	0.0689 - 0.0083i
TOC1 protein nucleus		

Chemical Species	F20014	O2015
<i>LHY</i> mRNA	-0.0966 - 0.0447i	-0.0472 - 0.3212i
LHY protein cytoplasm	-0.0678 - 0.0001i	-0.0379 - 0.1987i
LHY protein nucleus		-0.0500 - 0.1490i
<i>TOC1</i> mRNA	0.1067 + 0.0126i	0.1031 + 0.1951i
TOC1 protein cytoplasm	0.2552 - 0.1780i	1.0000 + 0.0000i
TOC1 protein nucleus	0.0338 - 0.0228i	0.0035 - 0.1787i

TABLE S23: Eigenvector entries for the mRNA and proteins of *LHY/CCA1* and *TOC1* genes under perpetual darkness continued. Empty entries are due to different definitions of variables.

Chemical Species	F2016	DC2016
<i>LHY</i> mRNA	-0.1706 + 0.4737i	1.0000 + 0.0000i
LHY protein	0.0871 + 0.5645i	0.7818 - 0.5124i
<i>TOC1</i> mRNA	0.0835 - 0.6265i	-0.2667 + 0.7053i
TOC1 protein	-0.3524 - 0.4064i	0.2779 + 0.6823i

TABLE S24: Eigenvector entries for the mRNA and proteins of *LHY/CCA1* and *TOC1* genes under perpetual darkness continued. F2016 and DC2016 models use only one variable for proteins of *LHY* and *TOC1*. The *TOC1* entries represent *PRR5/TOC1* gene group.

Model Idiosyncrasies

Model	ODE Solver	Comments
L2005a [2]	ode15s	The set of parameter values for optimal solution from Fig. 5 in Locke et al. 2005a is used for obtaining data in Fig. 3 in the main text and supplementary Figs. S13, S14a and S15a. The set of parameter values for a typical annealed solution from Fig. 4 in Locke et al. 2005a is used for obtaining data in supplementary Figs. S1 and S8. Parameters q_1 and q_2 are used with unit h^{-1} , and p_3 with unit nM/h .
L2005b [3]	ode15s	Model Two (the interlocked feedback look model) is used in our analysis, since it adds an extra loop to Model One as an improvement.
Z2006 [4]	ode15s	$PRR7 - PRR9light - Y'$ model is used in our analysis. In $PRR7 - PRR9light - Y'$ model, in equation of $\frac{dc_Y^{(m)}}{dt}$, term $c_L^{(n)fi}$ is interpreted as $c_L^{(n)i}$ as in $PRR7 - PRR9 - Y$ model.
P2010 [5]	ode15s	Model uses dimensionless chemical levels. L is set to 1 for perpetual illumination, and 0 for perpetual darkness in our analysis.
P2012 [6]	ode15s	Model uses dimensionless chemical levels. L is set to 1 for perpetual illumination, and 0 for perpetual darkness in our analysis. We added $c_{Ltot} = c_L + c_{Lmod}$, and interpret c_G in Eqs.(25)(26) as c_{Gc} .
P2013 [7]	ode15s	Use dimensionless chemical levels. L is set to 1 for perpetual illumination, and 0 for perpetual darkness in our analysis. Equations for HY5 and HFR1 proteins are not included since they are only used for optimization of $COP1$ parameters and are decoupled from other equations. We added $c_{Ltot} = c_L + c_{Lmod}$. We redefined c_{Gn} to be $c_{Gn} = p_{28}c_{Gc}/(p_{29} + m_{19} + p_{17}c_{E3n})$; and c_{AR} to be $c_{AR} = 0.5 \cdot (A_0 + c_{ABAR}^m + g_{29} - \sqrt{(A_0 + c_{ABAR}^m + g_{29}) + 4A_0c_{ABAR}^m})$.
F2014 [8]	ode15s	Use dimensionless chemical levels. The model is situated very close to another bifurcation at a lower degradation rate value under perpetual illumination. We interpret c_{Tn} in Eq. (18) as c_{Tn} .
O2015 [9]	ode15s	All the Θ terms are set to 1 for perpetual illumination, and 0 for perpetual darkness in our analysis.
F2016 [10]	ode23	Use dimensionless chemical levels. The kernel model is used in our analysis. The indexing and notations of parameters used in code given and the ones in main body of the original paper differs, and we followed the convention in the code provided ($\phi_7 \rightarrow \phi_{75}$, $\phi_8 \rightarrow \phi_{76}$, $\phi_9 \rightarrow \phi_{77}$, and $\phi_n \rightarrow \phi_{n-3}$ for $n \geq 10$. $\theta_{144} \rightarrow \phi_{71}$, $\theta_{145} \rightarrow \phi_{72}$).
DC2016 [11]	ode15s	We did not include the PIF gene, which controls the hypocotyl growth, since this gene is decoupled from the rest of the network and is not of special interests for our purposes. The model is situated very close to another bifurcation at a lower degradation rate value under perpetual darkness. We interpret $[P]_p$ in Eq. (3) as $[P]$; and P in Eq. (9) as the concentration $[P]$.

TABLE S25: Details and modifications to each model in our simulations and analysis.

S26 Response Curves

In this subsection we show amplitude response curves for systems that are either pre-bifurcation or post-bifurcation. To enable comparisons to experiments, results for both sinusoidal and square-wave forcing functions are shown.

To put the Stuart-Landau equation in a form useful to compute periodic forcing [12] and to generalize Eqs. (7) and (8) of the main text to the pre- and post-bifurcation regions, we make the a variable changes

$$\begin{aligned}
 \mu &\rightarrow \chi\mu \\
 \lambda_1 &\rightarrow \chi\lambda_1 \\
 W &\rightarrow (\chi\mu)^{-\frac{1}{2}} W' e^{-i\omega_0 t}
 \end{aligned} \tag{1}$$

where $\chi \equiv \text{sign}(\mu)$. Upon substitution of the scaled variables in Eqs. (1) and the addition of a forcing function $F(\omega t)$ with frequency ω , we find

$$\frac{dW'}{dt} = [\mu\sigma_1 + i(\omega_0 + \mu\omega_1)] W' - (g' + ig'') |W'|^2 W' + F(\omega t) \tag{2}$$

In the absence of forcing, the asymptotic free-running frequency is given by

$$\omega_s = \begin{cases} \omega_0 + \mu \left(\omega_1 - \frac{g''}{g'} \sigma_1 \right) & \text{for } \mu > 0, \\ \omega_0 + \mu \omega_1 & \text{for } \mu < 0 \end{cases} \quad (3)$$

Making another set of variable changes

$$\begin{aligned} t &\rightarrow \sigma_1^{-1} t' \\ \omega &\rightarrow \sigma_1 \omega' \\ \omega_s &\rightarrow \sigma_1 \omega'_s \\ W' &\rightarrow (\sigma_1/g')^{\frac{1}{2}} W'' e^{i\omega_s t} \\ F &\rightarrow (\sigma_1^3/g')^{\frac{1}{2}} F' \end{aligned} \quad (4)$$

non-dimensionalizes Eq. (2):

$$\frac{dW''}{dt} = \begin{cases} \left(1 + i \frac{g''}{g'}\right) \left(\mu W'' - |W''|^2 W''\right) + F'(\omega' t') e^{-i\omega'_s t'} & \text{for } \mu > 0 \\ \mu W'' - \left(1 + i \frac{g''}{g'}\right) |W''|^2 W'' + F'(\omega' t') e^{-i\omega'_s t'} & \text{for } \mu < 0 \end{cases} \quad (5)$$

To predict the response of the *Arabidopsis* circadian rhythm, we numerically compute the solutions to Eq. (5). Then, as a measure of the size of the response, we calculate the quantity $R \equiv \lim_{t \rightarrow \infty} \sqrt{\langle |W|^2 \rangle}$, where the angle brackets denote time average. Results are shown for sinusoidal forcing: $F'(\omega' t') = |F'| e^{i\omega' t'}$ and for square wave forcing: $F'(\omega' t') = 2|F'| \llbracket \omega' t' / \pi \rrbracket \pmod{2}$, for a range of $|F'|$ from 10^{-3} to 10^3 . We set the constants in Eq. (5) to correspond to typical values from the models: $\mu = 0.5$, $g'/g'' = 1$, $\omega'_s = 30$. We also set $\omega' = 30$ to force the system at the asymptotic free-running frequency. The resulting response curves are shown in Fig. S26. Fig. S26a shows the results for square-wave forcing, and Fig. S26b for sinusoidal forcing. The results indicate for weak forcing, i.e., where the dimensionless amplitude of the forcing function is small relative to the dimensionless limit-cycle amplitude, a pre-bifurcation system exhibits a linear response while a post-bifurcation exhibits no response. The maximum forcing amplitude that constitutes the upper bound of the “weak” regime is significantly larger for a square-wave forcing function. An experiment may be able to measure the response of the system to weak values of forcing to determine whether the system is pre-bifurcation or post-bifurcation.

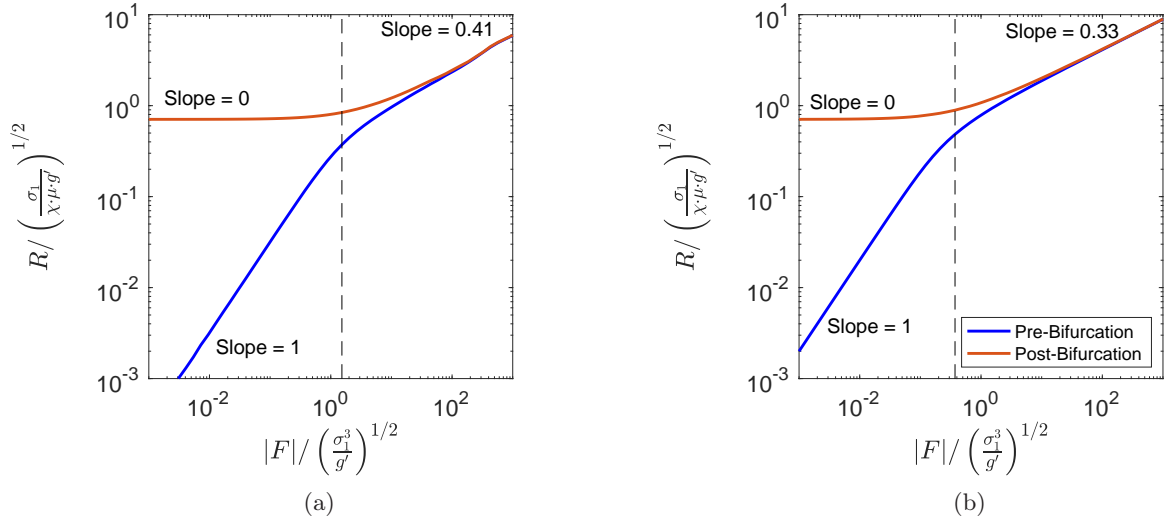


FIG. S26: Amplitude response curves for (a) square-wave forcing and (b) sinusoidal forcing. The vertical black dotted line indicates the visually estimated crossover value where the “weak-forcing” regime where $R \propto F^1$ (pre-bifurcation) or $R \propto F^0$ (post-bifurcation) changes to a “strong-forcing” regime where $R \propto F^n$ where $n = 0.41$ (square-wave) or $n = 0.33$ (sinusoidal).

-
- [1] Y. Kuramoto, *Chemical oscillations, waves, and turbulence* (Springer-Verlag, Berlin, Heidelberg, 1984).
 - [2] J. C. Locke, A. J. Millar, and M. S. Turner, Modelling genetic networks with noisy and varied experimental data: the circadian clock in *arabidopsis thaliana*, *Journal of theoretical biology* **234**, 383 (2005).
 - [3] J. C. Locke, M. M. Southern, L. Kozma-Bognár, V. Hibberd, P. E. Brown, M. S. Turner, and A. J. Millar, Extension of a genetic network model by iterative experimentation and mathematical analysis, *Molecular systems biology* **1**, 0013 (2005).
 - [4] M. N. Zeilinger, E. M. Farré, S. R. Taylor, S. A. Kay, and F. J. Doyle, A novel computational model of the circadian clock in *arabidopsis* that incorporates *prp7* and *prp9*, *Molecular Systems Biology* **2**, 58 (2006).
 - [5] A. Pokhilko, S. K. Hodge, K. Stratford, K. Knox, K. D. Edwards, A. W. Thomson, T. Mizuno, and A. J. Millar, Data assimilation constrains new connections and components in a complex, eukaryotic circadian clock model, *Molecular systems biology* **6**, 416 (2010).
 - [6] A. Pokhilko, A. P. Fernández, K. D. Edwards, M. M. Southern, K. J. Halliday, and A. J. Millar, The clock gene circuit in *arabidopsis* includes a repressilator with additional feedback loops, *Molecular systems biology* **8**, 574 (2012).
 - [7] A. Pokhilko, P. Mas, and A. J. Millar, Modelling the widespread effects of *toc1* signalling on the plant circadian clock and its outputs, *BMC systems biology* **7**, 23 (2013).
 - [8] K. Fogelmark and C. Troein, Rethinking transcriptional activation in the *arabidopsis* circadian clock, *PLoS computational biology* **10**, e1003705 (2014).
 - [9] T. Ohara, H. Fukuda, and I. T. Tokuda, An extended mathematical model for reproducing the phase response of *arabidopsis thaliana* under various light conditions, *Journal of theoretical biology* **382**, 337 (2015).
 - [10] M. Foo, D. E. Somers, and P.-J. Kim, Kernel architecture of the genetic circuitry of the *arabidopsis* circadian system, *PLoS computational biology* **12**, e1004748 (2016).
 - [11] J. De Caluwé, Q. Xiao, C. Hermans, N. Verbruggen, J.-C. Leloup, and D. Gonze, A compact model for the complex plant circadian clock, *Frontiers in plant science* **7**, 74 (2016).
 - [12] P. Le Gal, A. Nadim, and M. Thompson, Hysteresis in the forced stuart–landau equation: application to vortex shedding from an oscillating cylinder, *Journal of fluids and structures* **15**, 445 (2001).